

Temperature-dependent cross sections for charmonium dissociation in collisions with kaons and η mesons in hadronic matter

Shi-Tao Ji, Zhen-Yu Shen, Xiao-Ming Xu

Department of Physics, Shanghai University, Baoshan, Shanghai 200444, China

Abstract

We study kaon-charmonium and η -charmonium dissociation reactions. The K -charmonium dissociation and the η -charmonium dissociation include the following 27 reactions: $KJ/\psi \rightarrow \bar{D}^*D_s^+$, $\bar{D}D_s^{*+}$ and $\bar{D}^*D_s^{*+}$; $K\psi' \rightarrow \bar{D}^*D_s^+$, $\bar{D}D_s^{*+}$ and $\bar{D}^*D_s^{*+}$; $K\chi_c \rightarrow \bar{D}^*D_s^+$, $\bar{D}D_s^{*+}$ and $\bar{D}^*D_s^{*+}$; $\eta J/\psi \rightarrow \bar{D}^*D$, $\bar{D}D^*$, \bar{D}^*D^* , $D_s^{*-}D_s^+$, $D_s^-D_s^{*+}$ and $D_s^{*-}D_s^{*+}$; $\eta\psi' \rightarrow \bar{D}^*D$, $\bar{D}D^*$, \bar{D}^*D^* , $D_s^{*-}D_s^+$, $D_s^-D_s^{*+}$ and $D_s^{*-}D_s^{*+}$; $\eta\chi_c \rightarrow \bar{D}^*D$, $\bar{D}D^*$, \bar{D}^*D^* , $D_s^{*-}D_s^+$, $D_s^-D_s^{*+}$ and $D_s^{*-}D_s^{*+}$. Cross sections for the reactions are calculated in the Born approximation, in the quark-interchange mechanism and with a temperature-dependent quark potential. The temperature dependence of peak cross sections of endothermic reactions is linked to the temperature dependence of quark-antiquark relative-motion wave functions, meson masses and the quark potential. Although the η meson and kaon have similar masses, the energy and temperature dependence of the η -charmonium dissociation cross sections are quite different from those of the K -charmonium dissociation cross sections. Using the η -charmonium and π -charmonium dissociation cross sections, we calculate the ratio of the corresponding dissociation rates in hadronic matter and we find that such rates are comparable at low J/ψ momenta.

Keywords: Charmonium dissociation cross sections; quark-interchange mechanism

PACS: 25.75.-q; 24.85.+p; 12.38.Mh

1 Introduction

Nucleon- J/ψ dissociation cross sections have been calculated in Refs. [1, 2] from the gluon- J/ψ dissociation cross section obtained in short-distance QCD. J/ψ can be dissociated by a gluon with energy larger than the quark-antiquark binding energy of J/ψ [1–3]. As the nucleon energy increases, it generates an increasing number of gluons overcoming the binding so that J/ψ can be dissociated more easily. Therefore, the nucleon- J/ψ dissociation cross section increases with total energy of N and J/ψ in the centre-of-mass frame. This is a result of the short-distance approach in which the operator product expansion of perturbative QCD is applied to heavy quarkonia of small sizes [1, 2]. A similar energy dependence of $N + J/\psi$ and $\pi + J/\psi$ dissociation cross sections has been obtained in Ref. [4] despite hadron mass corrections to the cross-section formula of Peskin and Bhanot.

Including the Coulomb potential, the Fermi contact term acting as the spin-spin interaction and a colour-independent confining force active only between a quark and an antiquark, cross sections for $\pi + J/\psi \rightarrow \bar{D}^* + D$, $\pi + J/\psi \rightarrow \bar{D} + D^*$ and $\pi + J/\psi \rightarrow \bar{D}^* + D^*$ have been calculated in Ref. [5] in the quark-interchange mechanism [6, 7]. The colour interaction that includes the colour Coulomb, spin-spin hyperfine and linear confining interactions has been considered in Refs. [8, 9] for the dissociation of charmonia in collisions with π and ρ mesons. These quark-model calculations of the quark-interchange mechanism give the result that the cross section increases from a threshold energy for every endothermic reaction from zero, reaching a maximum and decreasing with total energy of the meson and charmonium in the centre-of-mass frame. This is the energy dependence of the cross section obtained in the quark-interchange approach of the quark potential models [5–9], where the quark interchange mechanism between the two initial mesons breaks the charmonium.

A study of $\pi + J/\psi \rightarrow \bar{D}^* + D$, $\pi + J/\psi \rightarrow \bar{D} + D^*$ and $\rho + J/\psi \rightarrow \bar{D} + D$ at low energies of the mesons was initiated in Ref. [10]. Meson exchange between the two initial mesons breaks the charmonium and Lagrangians with meson couplings are constructed to describe

the motion of meson fields. This is the essence of the meson-exchange approach [10–16]. Effective meson Lagrangians with different symmetries lead to different cross sections for the same reaction [11–16]. Near threshold energies cross sections increase for endothermic reactions and decrease for exothermic reactions. When the total energy of the two initial mesons in the centre-of-mass frame rises far away from threshold, the increase or decrease of the cross sections is due to form factors inserted in three-meson and four-meson vertices of Feynman diagrams.

The energy dependence of cross sections for some hadron-charmonium dissociation reactions in vacuum has been studied in the short-distance, the meson-exchange and the quark-interchange approaches. In hadronic matter not only the energy dependence is interesting, but also the temperature dependence of hadron-charmonium dissociation cross sections is important [17]. From vacuum to hadronic matter the quark potential, mesonic quark-antiquark relative-motion wave functions, meson masses and cross sections for π -charmonium and ρ -charmonium dissociation change significantly. The temperature dependence of the cross sections has been shown to be unexpected [18]. For instance, even though a ρ -charmonium reaction is exothermic in vacuum, it may be endothermic in hadronic matter; the peak cross section of any π -charmonium dissociation reaction first decreases with increasing temperature, but then increases rapidly when the temperature approaches the critical temperature. Therefore, we continue here the study of temperature dependence. We choose kaon-charmonium dissociation reactions as the first objective of the present work. The energy dependence of the cross sections for the reactions in vacuum has been studied in Ref. [8], but in hadronic matter it is not available. The temperature dependence of the kaon-charmonium dissociation cross sections has not been studied either.

It has been shown by experiments that the ratios K^+/π^+ , K^-/π^- and η/π^0 at midrapidity increase with increasing transverse momentum p_T and the increase is visible only in a certain range of transverse momentum. For central Au+Au collisions at $\sqrt{s_{NN}} = 200$ GeV the ratio K^+/π^+ (K^-/π^-) measured by the PHENIX Collaboration is available from $p_T = 0.45$ GeV/ c to 1.95 GeV/ c and it is 0.234 (0.221) at $p_T = 0.65$ GeV/ c and 0.55 (0.55)

at $p_T = 1.65$ GeV/ c at midrapidity [19]. For central Pb+Pb collisions at $\sqrt{s_{NN}} = 2.76$ TeV the ratio $(K^+ + K^-)/(\pi^+ + \pi^-)$ measured by the ALICE Collaboration increases with increasing transverse momentum from $p_T = 0$, forms a peak at $p_T \approx 3$ GeV/ c and goes to the value 0.45 at $p_T > 4$ GeV/ c [20]. At present, for central Au+Au collisions at $\sqrt{s_{NN}} = 200$ GeV the smallest η transverse momentum measured by the PHENIX Collaboration is 1.65 GeV/ c and the ratio η/π^0 is 0.46 at $p_T = 1.65$ GeV/ c at midrapidity [21]. From the measured ratios we conclude that the η species is as rich as the K^+ and K^- species in hadronic matter and we need to study η -charmonium dissociation reactions which form the second objective of the present work. The short-distance approach and the quark-interchange approach have not been studied for the η -charmonium dissociation reactions. The $\eta + J/\psi$ dissociation in vacuum was considered in Ref. [12], but no cross sections were presented. However, we will show that $\eta + J/\psi$ dissociation reactions need to be considered in the study of J/ψ suppression in hadronic matter.

This paper is organized as follows. In the next section we present cross-section formulas for the charmonium dissociation in collision with a meson. In Section 3 kaon-charmonium and η -charmonium dissociation reactions are listed, numerical cross sections are shown, relevant discussions are given and the numerical results are parametrized in Appendix A. Using the η -charmonium dissociation cross sections and the π -charmonium dissociation cross sections given in Ref. [18], we calculate the ratio of the corresponding dissociation rates in hadronic matter. A summary is in the last section.

2 Cross-section formulas

In quark degrees of freedom the meson-charmonium dissociation is expressed as $q\bar{q} + c\bar{c} \rightarrow q\bar{c} + c\bar{q}$ where q stands for the up quark, down quark or strange quark. The flavour of the quark q may be different from the flavour of the antiquark \bar{q} . The cross section for $q\bar{q} + c\bar{c} \rightarrow q\bar{c} + c\bar{q}$ is [22]

$$\sigma(S, m_S, \sqrt{s}, T) = \frac{1}{32\pi s} \frac{|\vec{P}'(\sqrt{s})|}{|\vec{P}(\sqrt{s})|} \int_0^\pi d\theta |\mathcal{M}_{\bar{q}}(s, t)|^2 \sin \theta, \quad (1)$$

where S is the total spin of either the two initial mesons or the two final mesons, and it is conserved in the reaction; m_S denotes the magnetic projection quantum number of the total spin. The Mandelstam variables are $s = (E_{q\bar{q}} + E_{c\bar{c}})^2 - (\vec{P}_{q\bar{q}} + \vec{P}_{c\bar{c}})^2$ and $t = (E_{q\bar{q}} - E_{q\bar{c}})^2 - (\vec{P}_{q\bar{q}} - \vec{P}_{q\bar{c}})^2$, where $P_i = (E_i, \vec{P}_i)$ is the four-momentum of meson i ($i = q\bar{q}, c\bar{c}, q\bar{c}, c\bar{q}$); θ is the angle between the three-dimensional $q\bar{q}$ momentum \vec{P} and the three-dimensional $q\bar{c}$ momentum \vec{P}' in the centre-of-mass frame.

\mathcal{M}_{fi} in Eq. (1) stands for the transition amplitude, which takes different values for the two forms of meson-meson scattering, namely, the prior form in Fig. 1 and the post form in Fig. 2 [23–25]. The scattering in the prior form means that gluon exchange occurs before quark interchange. The corresponding transition amplitude is

$$\mathcal{M}_{\text{fi}}^{\text{prior}} = 4\sqrt{E_{q\bar{q}}E_{c\bar{c}}E_{q\bar{c}}E_{c\bar{q}}}\langle\psi_{q\bar{c}}|\langle\psi_{c\bar{q}}|(V_{q\bar{c}} + V_{c\bar{q}} + V_{qc} + V_{\bar{q}\bar{c}})|\psi_{q\bar{q}}\rangle|\psi_{c\bar{c}}\rangle, \quad (2)$$

where the meson wave functions, $\psi_{q\bar{c}}$, $\psi_{c\bar{q}}$, $\psi_{q\bar{q}}$ and $\psi_{c\bar{c}}$, represent the products of quark-antiquark relative-motion wave functions in momentum space and wave functions in the colour space, spin space and flavour space. $V_{q\bar{c}}$ is the potential of q and \bar{c} and the meaning of $V_{c\bar{q}}$ and so on can be understood in the same way. The scattering in the post form contains gluon exchange after quark interchange. The corresponding transition amplitude is

$$\mathcal{M}_{\text{fi}}^{\text{post}} = 4\sqrt{E_{q\bar{q}}E_{c\bar{c}}E_{q\bar{c}}E_{c\bar{q}}}\langle\psi_{q\bar{c}}|\langle\psi_{c\bar{q}}|(V_{q\bar{q}} + V_{c\bar{c}} + V_{qc} + V_{\bar{q}\bar{c}})|\psi_{q\bar{q}}\rangle|\psi_{c\bar{c}}\rangle. \quad (3)$$

The potential in momentum space in Eqs. (2) and (3) is the Fourier transform of the potential provided in Ref. [18],

$$V_{ab}(\vec{r}) = V_{\text{si}}(\vec{r}) + V_{\text{ss}}(\vec{r}), \quad (4)$$

where $V_{\text{si}}(\vec{r})$ is a central spin-independent potential and $V_{\text{ss}}(\vec{r})$ is a spin-spin interaction. The temperature dependence is explicitly expressed in $V_{\text{si}}(\vec{r})$,

$$V_{\text{si}}(\vec{r}) = -\frac{\vec{\lambda}_a}{2} \cdot \frac{\vec{\lambda}_b}{2} \frac{3}{4} D \left[1.3 - \left(\frac{T}{T_c} \right)^4 \right] \tanh(Ar) + \frac{\vec{\lambda}_a}{2} \cdot \frac{\vec{\lambda}_b}{2} \frac{6\pi}{25} \frac{v(\lambda r)}{r} \exp(-Er), \quad (5)$$

where $D = 0.7$ GeV, $T_c = 0.175$ GeV, $A = 1.5[0.75 + 0.25(T/T_c)^{10}]^6$ GeV, $E = 0.6$ GeV and $\lambda = \sqrt{3b_0/16\pi^2\alpha'}$ in which $\alpha' = 1.04$ GeV⁻² and $b_0 = 11 - \frac{2}{3}N_f$ with $N_f = 4$; $\vec{\lambda}_a$

are the Gell-Mann matrices for the colour generators of constituent a . The dimensionless function $v(x)$ [26] is

$$v(x) = \frac{4b_0}{\pi} \int_0^\infty \frac{dQ}{Q} \left[\rho(\vec{Q}^2) - \frac{K}{\vec{Q}^2} \right] \sin\left(\frac{Q}{\lambda}x\right), \quad (6)$$

where $K = 3/16\pi^2\alpha'$ and $\rho(\vec{Q}^2)$ is the physical running coupling constant at the gluon momentum \vec{Q} .

Lattice QCD calculations gave a temperature-dependent quark potential at intermediate and large distances [27]. In contrast to the linear confinement in vacuum, the quark potential at large distances is independent of the distance and is a plateau. With increasing temperature the plateau becomes lower and lower and confinement gets weaker and weaker. From a large distance to an intermediate distance the variation of the potential with respect to temperature gets smaller. At $r \approx 0.3$ fm the variation disappears. The lattice QCD results (the above potential) [27] give the spin-independent potential in Eq. (5) at intermediate and large distances. At short distances quark interaction is described by perturbative QCD in vacuum. The spin-independent potential in Eq. (5) at short distances is thus given by one-gluon exchange plus perturbative one- and two-loop corrections in vacuum [26]. The temperature dependence of the potential in Eq. (5) comes from the lattice QCD results. The potential well fits the lattice QCD results at $T/T_c > 0.55$ [28] and is constrained by perturbative QCD at short distances and the lattice QCD results at intermediate and large distances. We may adjust the parameters A and E to get a good fit of the lattice QCD results, for example, reduce A by 5% and increase E by 10% or increase A by 5% and reduce E by 10%. But the changes of the two parameters lead to very small changes of meson masses and cross sections for meson-meson reactions [28]. Hence, the potential has the uncertainty of the values of A and E , but the uncertainty causes very small changes in meson mass and in cross section. The expression $\frac{\bar{\lambda}_a}{2} \cdot \frac{\bar{\lambda}_b}{2} \frac{6\pi}{25} \frac{v(\lambda r)}{r}$ in the second term of Eq. (5) is obtained in perturbative QCD and arises from one-gluon exchange plus perturbative one- and two-loop corrections in vacuum [26]. The factor $\exp(-Er)$ assures that the potential at small distances is given by perturbative QCD in vacuum. The second term in Eq. (5) is independent of temperature.

From a correlator of a very heavy quark-antiquark pair a time-dependent potential was obtained in quenched lattice QCD [29, 30]. Only at very large times and at $T < T_c$ the potential agrees with the free energy in the Coulomb gauge. Using the free energy from lattice calculations as the potential of a charm quark and a charm antiquark in the Schrödinger equation correctly describes the nonrelativistic wave function of J/ψ and reproduces the J/ψ mass from the QCD sum rule in the vicinity of the critical temperature [31]. When the system's temperature is smaller than the critical temperature, the product of the temperature and a meson's entropy is small or negligible in comparison with the quark-antiquark free energy and the free energy can be taken as the quark-antiquark potential to a good approximation [32]. The three methods suggest that the free energy obtained in the lattice QCD calculations can be taken as the quark potential in hadronic matter.

The spin-spin interaction $V_{ss}(\vec{r})$ arises from perturbative one-gluon exchange plus one- and two-loop corrections [33] and includes relativistic effects [7, 9, 34]:

$$V_{ss}(\vec{r}) = -\frac{\vec{\lambda}_a \cdot \vec{\lambda}_b}{2} \cdot \frac{16\pi^2}{25} \frac{d^3}{\pi^{3/2}} \exp(-d^2 r^2) \frac{\vec{s}_a \cdot \vec{s}_b}{m_a m_b} + \frac{\vec{\lambda}_a \cdot \vec{\lambda}_b}{2} \cdot \frac{4\pi}{25} \frac{1}{r} \frac{d^2 v(\lambda r)}{dr^2} \frac{\vec{s}_a \cdot \vec{s}_b}{m_a m_b}, \quad (7)$$

where \vec{s}_a and m_a are the spin and mass of constituent a , respectively, and the quantity d is related to quark masses by

$$d^2 = \sigma_0^2 \left[\frac{1}{2} + \frac{1}{2} \left(\frac{4m_a m_b}{(m_a + m_b)^2} \right)^4 \right] + \sigma_1^2 \left(\frac{2m_a m_b}{m_a + m_b} \right)^2, \quad (8)$$

where $\sigma_0 = 0.15$ GeV and $\sigma_1 = 0.705$.

Finally, the unpolarised cross section is

$$\begin{aligned} \sigma^{\text{unpol}}(\sqrt{s}, T) &= \frac{1}{(2S_{q\bar{q}} + 1)(2S_{c\bar{c}} + 1)(2L_{c\bar{c}} + 1)} \sum_{SL_{c\bar{c}z}} (2S + 1) \\ &\times \frac{\sigma^{\text{prior}}(S, m_S, \sqrt{s}, T) + \sigma^{\text{post}}(S, m_S, \sqrt{s}, T)}{2}, \end{aligned} \quad (9)$$

where $S_{q\bar{q}}$ ($S_{c\bar{c}}$) is the $q\bar{q}$ ($c\bar{c}$) spin and σ^{prior} (σ^{post}) is obtained by the replacement of \mathcal{M}_{fi} in Eq. (1) by $\mathcal{M}_{\text{fi}}^{\text{prior}}$ ($\mathcal{M}_{\text{fi}}^{\text{post}}$). $L_{c\bar{c}z}$ is the magnetic projection quantum number of the orbital angular momentum $L_{c\bar{c}}$ of the meson $c\bar{c}$.

3 Reactions, results and discussions

Given the charm quark mass $m_c = 1.51$ GeV, the up and down quark masses $m_u = m_d = 0.32$ GeV and the strange quark mass $m_s = 0.5$ GeV, the Schrödinger equation with the potential in Eq. (4) at $T = 0$ reproduces [18] the experimental masses of J/ψ , ψ' , χ_c , the pion, the rho, the kaon, the vector kaon, the η meson, the charmed mesons and the charmed strange mesons [35]. The potential at $T = 0$ and the mesonic quark-antiquark relative-motion wave functions obtained from the Schrödinger equation reproduce the experimental data of S -wave $I = 2$ elastic phase shifts for $\pi\pi$ scattering in vacuum [36–39].

3.1 Dissociation reactions

We establish the notation $K = \begin{pmatrix} K^+ \\ K^0 \end{pmatrix}$, $\bar{K} = \begin{pmatrix} \bar{K}^0 \\ K^- \end{pmatrix}$, $D = \begin{pmatrix} D^+ \\ D^0 \end{pmatrix}$, $\bar{D} = \begin{pmatrix} \bar{D}^0 \\ D^- \end{pmatrix}$, $D^* = \begin{pmatrix} D^{*+} \\ D^{*0} \end{pmatrix}$ and $\bar{D}^* = \begin{pmatrix} \bar{D}^{*0} \\ D^{*-} \end{pmatrix}$. The K -charmonium dissociation includes the reactions:

$$\begin{aligned} K + J/\psi &\rightarrow \bar{D}^* + D_s^+, & K + J/\psi &\rightarrow \bar{D} + D_s^{*+}, & K + J/\psi &\rightarrow \bar{D}^* + D_s^{*+}, \\ K + \psi' &\rightarrow \bar{D}^* + D_s^+, & K + \psi' &\rightarrow \bar{D} + D_s^{*+}, & K + \psi' &\rightarrow \bar{D}^* + D_s^{*+}, \\ K + \chi_c &\rightarrow \bar{D}^* + D_s^+, & K + \chi_c &\rightarrow \bar{D} + D_s^{*+}, & K + \chi_c &\rightarrow \bar{D}^* + D_s^{*+}. \end{aligned}$$

The \bar{K} -charmonium dissociation includes

$$\begin{aligned} \bar{K} + J/\psi &\rightarrow D_s^{*-} + D, & \bar{K} + J/\psi &\rightarrow D_s^- + D^*, & \bar{K} + J/\psi &\rightarrow D_s^{*-} + D^*, \\ \bar{K} + \psi' &\rightarrow D_s^{*-} + D, & \bar{K} + \psi' &\rightarrow D_s^- + D^*, & \bar{K} + \psi' &\rightarrow D_s^{*-} + D^*, \\ \bar{K} + \chi_c &\rightarrow D_s^{*-} + D, & \bar{K} + \chi_c &\rightarrow D_s^- + D^*, & \bar{K} + \chi_c &\rightarrow D_s^{*-} + D^*. \end{aligned}$$

Cross sections for the \bar{K} – charmonium dissociation reactions are obtained from the K – charmonium dissociation reactions, for instance, the cross section for $\bar{K} + J/\psi \rightarrow D_s^- + D^*$ is identical to the cross section for $K + J/\psi \rightarrow \bar{D}^* + D_s^+$. Since the η meson has the

components of $u\bar{u}$, $d\bar{d}$ and $s\bar{s}$, the η -charmonium dissociation includes $u\bar{u}$ - or $d\bar{d}$ -induced reactions, viz.

$$\begin{aligned}\eta + J/\psi &\rightarrow \bar{D}^* + D, & \eta + J/\psi &\rightarrow \bar{D} + D^*, & \eta + J/\psi &\rightarrow \bar{D}^* + D^*, \\ \eta + \psi' &\rightarrow \bar{D}^* + D, & \eta + \psi' &\rightarrow \bar{D} + D^*, & \eta + \psi' &\rightarrow \bar{D}^* + D^*, \\ \eta + \chi_c &\rightarrow \bar{D}^* + D, & \eta + \chi_c &\rightarrow \bar{D} + D^*, & \eta + \chi_c &\rightarrow \bar{D}^* + D^*,\end{aligned}$$

and $s\bar{s}$ -induced reactions,

$$\begin{aligned}\eta + J/\psi &\rightarrow D_s^{*-} + D_s^+, & \eta + J/\psi &\rightarrow D_s^- + D_s^{*+}, & \eta + J/\psi &\rightarrow D_s^{*-} + D_s^{*+}, \\ \eta + \psi' &\rightarrow D_s^{*-} + D_s^+, & \eta + \psi' &\rightarrow D_s^- + D_s^{*+}, & \eta + \psi' &\rightarrow D_s^{*-} + D_s^{*+}, \\ \eta + \chi_c &\rightarrow D_s^{*-} + D_s^+, & \eta + \chi_c &\rightarrow D_s^- + D_s^{*+}, & \eta + \chi_c &\rightarrow D_s^{*-} + D_s^{*+}.\end{aligned}$$

The valence quark-antiquark wave function of the η meson is

$$\psi_\eta = \frac{1}{\sqrt{6}}\phi_{u\bar{u}}\phi_C\phi_S u\bar{u} + \frac{1}{\sqrt{6}}\phi_{d\bar{d}}\phi_C\phi_S d\bar{d} - \frac{2}{\sqrt{6}}\phi_{s\bar{s}}\phi_C\phi_S s\bar{s}, \quad (10)$$

where $\phi_{u\bar{u}}$ ($\phi_{d\bar{d}}$, $\phi_{s\bar{s}}$) is the relative-motion wave function of the up (down, strange) quark and the up (down, strange) antiquark in momentum space; ϕ_C and ϕ_S are the colour wave function and the spin wave function, respectively. $\phi_{u\bar{u}}$, $\phi_{d\bar{d}}$ and $\phi_{s\bar{s}}$ satisfy

$$\int \frac{d^3 p_{u\bar{u}}}{(2\pi)^3} \phi_{u\bar{u}}^*(\vec{p}_{u\bar{u}}) \phi_{u\bar{u}}(\vec{p}_{u\bar{u}}) = \int \frac{d^3 p_{d\bar{d}}}{(2\pi)^3} \phi_{d\bar{d}}^*(\vec{p}_{d\bar{d}}) \phi_{d\bar{d}}(\vec{p}_{d\bar{d}}) = \int \frac{d^3 p_{s\bar{s}}}{(2\pi)^3} \phi_{s\bar{s}}^*(\vec{p}_{s\bar{s}}) \phi_{s\bar{s}}(\vec{p}_{s\bar{s}}) = 1, \quad (11)$$

where $\vec{p}_{u\bar{u}}$ ($\vec{p}_{d\bar{d}}$, $\vec{p}_{s\bar{s}}$) is the relative momentum of the up (down, strange) quark and the up (down, strange) antiquark. The first (second, third) term is used in the transition amplitude to obtain the cross sections $\sigma_{\eta+c\bar{c}\rightarrow u\bar{c}+c\bar{u}}$ ($\sigma_{\eta+c\bar{c}\rightarrow d\bar{c}+c\bar{d}}$, $\sigma_{\eta+c\bar{c}\rightarrow s\bar{c}+c\bar{s}}$) for the $u\bar{u}$ -induced ($d\bar{d}$ -induced, $s\bar{s}$ -induced) reactions. The cross section for the η -charmonium dissociation is

$$\sigma_{\eta c\bar{c}} = \frac{1}{6}\sigma_{\eta+c\bar{c}\rightarrow u\bar{c}+c\bar{u}} + \frac{1}{6}\sigma_{\eta+c\bar{c}\rightarrow d\bar{c}+c\bar{d}} + \frac{2}{3}\sigma_{\eta+c\bar{c}\rightarrow s\bar{c}+c\bar{s}}. \quad (12)$$

The cross section for the production of \bar{D}^*D , $\bar{D}D^*$ or \bar{D}^*D^* equals the first and second terms while the one for the production of $D_s^{*-}D_s^+$, $D_s^-D_s^{*+}$ or $D_s^{*-}D_s^{*+}$ equals the third term.

3.2 Numerical cross sections and discussions

Solving the Schrödinger equation with the potential in Eq. (4), we obtain temperature-dependent meson masses shown in Figs. 1 and 17 in Ref. [18] and quark-antiquark relative-motion wave functions for charmonia, charmed mesons, charmed strange mesons and the mesons in the ground-state pseudoscalar octet and the ground-state vector nonet. The quark-antiquark relative-motion wave functions used in the transition amplitude are the Fourier transforms of the relative-motion wave functions obtained here. Since the up quark has the same mass as the down quark, $\phi_{u\bar{u}}$ equals $\phi_{d\bar{d}}$ but differs from $\phi_{s\bar{s}}$. Then, the cross sections $\sigma_{\eta+c\bar{c}\rightarrow u\bar{c}+c\bar{u}}$ for the $u\bar{u}$ -induced reactions are the same as $\sigma_{\eta+c\bar{c}\rightarrow d\bar{c}+c\bar{d}}$ for the $d\bar{d}$ -induced reactions.

Cross sections for exothermic reactions are infinite at threshold energies and we start calculating the cross sections at $\sqrt{s} = m_{q\bar{q}} + m_{c\bar{c}} + \Delta\sqrt{s}$ with $\Delta\sqrt{s} = 10^{-4}$ GeV. Unpolarised cross sections for the K -charmonium dissociation reactions and η -charmonium dissociation reactions are displayed in Figs. 3-23. The cross sections for exothermic reactions decrease very rapidly from infinity when \sqrt{s} increases from the threshold energies. To indicate this feature of an exothermic reaction, the rapid decrease should be displayed. However, when we start plotting the cross sections at the threshold energies plus 5×10^{-3} GeV, the decreasing part of the curve for $\eta + \chi_c \rightarrow \bar{D}^* + D$ at $T/T_c = 0.9$ in Fig. 16 disappears. Likewise when we start plotting the cross sections at the threshold energies plus 10^{-3} GeV, the decreasing part of the curve for $\eta + \psi' \rightarrow \bar{D}^* + D$ at $T/T_c = 0.65$ in Fig. 14 disappears. Therefore, we choose the threshold energies plus 10^{-4} GeV to start plotting the cross sections so that the rapid decrease is visible.

In vacuum the cross section for $KJ/\psi \rightarrow \bar{D}D_s^{*+}$ obtained from the effective meson Lagrangian in Ref. [12] increases with increasing \sqrt{s} and reaches a magnitude of about 8 mb. In the present work the cross section for $KJ/\psi \rightarrow \bar{D}D_s^{*+}$ shown by the curve at $T = 0$ first increases to a maximum value of about 0.27 mb with increasing \sqrt{s} and then decreases. Therefore, the magnitude of the present cross section is much smaller than the magnitude obtained in Ref. [12]. The $\eta J/\psi$ dissociation in vacuum was considered in

Ref. [12], but no cross sections were shown. In Ref. [8] cross sections for the production of $\bar{D}^*D_s^+$, $\bar{D}D_s^{*+}$ and $\bar{D}^*D_s^{*+}$ in the K -charmonium dissociation in vacuum were obtained in the quark-interchange mechanism. The peak cross section of the endothermic reaction $KJ/\psi \rightarrow \bar{D}^*D_s^+ + \bar{D}D_s^{*+} + \bar{D}^*D_s^{*+}$ is about 0.7 mb at the kinetic energy of the order of 0.44 GeV. The cross section for the exothermic reaction $K\psi' \rightarrow \bar{D}^*D_s^+ + \bar{D}D_s^{*+} + \bar{D}^*D_s^{*+}$ decreases very rapidly and then increases slowly to form a wide peak that corresponds to a cross section of about 1 mb. The exothermic reaction $K\chi_{c1} \rightarrow \bar{D}^*D_s^+ + \bar{D}D_s^{*+} + \bar{D}^*D_s^{*+}$ has a peak cross section of about 3 mb at the kinetic energy of the order of 0.17 GeV. By comparison, we obtain a peak cross section of about 0.6 mb at the kinetic energy of the order of 0.44 GeV for $KJ/\psi \rightarrow \bar{D}^*D_s^+ + \bar{D}D_s^{*+} + \bar{D}^*D_s^{*+}$, no peak cross section for $K\psi' \rightarrow \bar{D}^*D_s^+ + \bar{D}D_s^{*+} + \bar{D}^*D_s^{*+}$ and a peak cross section of about 3.4 mb at the kinetic energy of the order of 0.08 GeV for $K\chi_c \rightarrow \bar{D}^*D_s^+ + \bar{D}D_s^{*+} + \bar{D}^*D_s^{*+}$. We note that we use the average value of the χ_{c0} , χ_{c1} and χ_{c2} masses as the χ_c mass and the average value is a little higher than the χ_{c1} mass. The present results are comparable to the K -charmonium dissociation cross sections in Ref. [8]. The present work and the quark-interchange model in Ref. [8] have the same colour matrix elements and the same spin matrix elements, but have different quark potentials that lead to different spatial matrix elements in the transition amplitude. Hence, the energy dependence of the K -charmonium dissociation cross sections obtained in the present work is not the same as that displayed in Ref. [8].

In Figs. 3-11 only $K + \psi' \rightarrow \bar{D}^* + D_s^+$, $K + \psi' \rightarrow \bar{D} + D_s^{*+}$, $K + \psi' \rightarrow \bar{D}^* + D_s^{*+}$, $K + \chi_c \rightarrow \bar{D}^* + D_s^+$ and $K + \chi_c \rightarrow \bar{D} + D_s^{*+}$ at $T = 0$ are exothermic. While temperature goes from $0.65T_c$ to $0.75T_c$, the increases of the kaon and charmonium radii cause the increases of the peak cross sections of the $K + J/\psi$ and $K + \chi_c$ reactions, but the peak cross sections of the $K + \psi'$ reactions decrease. This relates to the node in the ψ' wave function. The node leads to cancellation between the negative wave function on the left of the node and the positive wave function on the right of the node in the integration involved in the transition amplitude. While the cancellation at $T = 0.75T_c$ is larger than at $T = 0.65T_c$, the peak cross sections of $K + \psi' \rightarrow \bar{D}^* + D_s^+$, $K + \psi' \rightarrow \bar{D} + D_s^{*+}$ and $K + \psi' \rightarrow \bar{D}^* + D_s^{*+}$ decrease from $T = 0.65T_c$ to $0.75T_c$. While temperature

increases from $T = 0.75T_c$, the increase of $|\mathcal{M}_{\bar{f}}|^2$ caused by the slow increases of the two initial-meson radii cannot overcome the reduction by the weakening confinement and the peak cross sections thus decrease. However, the rapid increases of the kaon and J/ψ radii from $T = 0.9T_c$ to $0.95T_c$ cause the increase of $|\mathcal{M}_{\bar{f}}|^2$ to overcome the reduction by the weakening confinement, and the peak cross sections of $K + J/\psi \rightarrow \bar{D}^* + D_s^+$, $K + J/\psi \rightarrow \bar{D} + D_s^{*+}$ and $K + J/\psi \rightarrow \bar{D}^* + D_s^{*+}$ rise rapidly from $T = 0.9T_c$ to $0.95T_c$.

We need to mention the difference between the cross section for $K + J/\psi \rightarrow \bar{D}^* + D_s^+$ and the one for $K + J/\psi \rightarrow \bar{D} + D_s^{*+}$. The difference arises from the different spins of the charmed mesons and the different spins of the charmed strange mesons between the two reactions. The masses of the \bar{D} , \bar{D}^* , D_s^+ and D_s^{*+} mesons are different and the sum of the \bar{D}^* and D_s^+ masses is smaller than the sum of the \bar{D} and D_s^{*+} masses. Hence, the endothermic reaction $K + J/\psi \rightarrow \bar{D}^* + D_s^+$ takes place more easily than $K + J/\psi \rightarrow \bar{D} + D_s^{*+}$ and at $T/T_c=0$ (0.65, 0.75, 0.85, 0.9, 0.95) the peak cross section of $K + J/\psi \rightarrow \bar{D}^* + D_s^+$ is 18% (47%, 42%, 11%, 135%, 95%) larger than the one of $K + J/\psi \rightarrow \bar{D} + D_s^{*+}$. The difference between the cross section for $K + \psi' \rightarrow \bar{D}^* + D_s^+$ and the one for $K + \psi' \rightarrow \bar{D} + D_s^{*+}$ ($K + \chi_c \rightarrow \bar{D}^* + D_s^+$ and $K + \chi_c \rightarrow \bar{D} + D_s^{*+}$) can be similarly understood.

The cross sections for the η -charmonium dissociation reactions have the following behaviour. As shown in Figs. 12-17, only three reactions $\eta + J/\psi \rightarrow \bar{D}^* + D$, $\eta + J/\psi \rightarrow \bar{D} + D^*$ and $\eta + J/\psi \rightarrow \bar{D}^* + D^*$ are endothermic below some temperature. The peak cross sections of the reactions increase with temperature from $T = 0$ to $0.85T_c$. As shown in Figs. 18-23, only three reactions $\eta + \psi' \rightarrow D_s^{*-} + D_s^+$, $\eta + \psi' \rightarrow D_s^- + D_s^{*+}$ and $\eta + \psi' \rightarrow D_s^{*-} + D_s^{*+}$ are exothermic below some temperature. The peak cross sections of the reactions decrease with temperature going from $T = 0.65T_c$ to T_c . The peak cross sections of $\eta + J/\psi \rightarrow D_s^{*-} + D_s^+$, $\eta + J/\psi \rightarrow D_s^- + D_s^{*+}$, $\eta + J/\psi \rightarrow D_s^{*-} + D_s^{*+}$, $\eta + \chi_c \rightarrow D_s^{*-} + D_s^+$, $\eta + \chi_c \rightarrow D_s^- + D_s^{*+}$ and $\eta + \chi_c \rightarrow D_s^{*-} + D_s^{*+}$ first rise and then fall with temperature increasing in the region $0 \leq T < T_c$.

Since the ratio of the η mass to the kaon mass is about 1.1 for $0 \leq T/T_c < 1$, i.e. the two masses are close, it is interesting to compare the peak cross sections of the

endothermic η -charmonium dissociation reactions with those of the endothermic kaon-charmonium dissociation reactions. The peak cross section of $\eta + J/\psi \rightarrow \bar{D}^* + D$ at $T/T_c = 0$ (0.65, 0.75, 0.85) is 1.64 (1.57, 1.55, 12.11) times the peak cross section of $K + J/\psi \rightarrow \bar{D}^* + D_s^+$ at the same temperature. The peak cross section of $\eta + J/\psi \rightarrow \bar{D}^* + D^*$ at $T/T_c = 0$ (0.65, 0.75, 0.85) is 0.56 (1.47, 3.87, 49.4) times the peak cross section of $K + J/\psi \rightarrow \bar{D}^* + D_s^{*+}$. This means that for $0.6 \leq T/T_c < 1$ the cross sections for $\eta + J/\psi \rightarrow \bar{D}^* + D$ and $\eta + J/\psi \rightarrow \bar{D}^* + D^*$ around their cross-section peaks are larger than the cross sections for $K + J/\psi \rightarrow \bar{D}^* + D_s^+$ and $K + J/\psi \rightarrow \bar{D}^* + D_s^{*+}$, respectively. Except for $\eta + J/\psi \rightarrow D_s^{*-} + D_s^{*+}$ and $K + J/\psi \rightarrow \bar{D}^* + D_s^{*+}$ at $T/T_c = 0.85$, the peak cross sections of $\eta + \text{charmonium} \rightarrow D_s^{*-} + D_s^+$ and $\eta + \text{charmonium} \rightarrow D_s^{*-} + D_s^{*+}$ are smaller than the ones of $K + \text{charmonium} \rightarrow \bar{D}^* + D_s^+$ and $K + \text{charmonium} \rightarrow \bar{D}^* + D_s^{*+}$, respectively.

Since the η -charmonium dissociation and the π -charmonium dissociation may produce the same charmed mesons, it is interesting to compare the peak cross sections of the endothermic η -charmonium dissociation reactions with those of endothermic π -charmonium dissociation reactions. Cross sections for the π -charmonium dissociation reactions are given in Ref. [18]. At any temperature between $T/T_c = 0.6$ and 1 the peak cross section of $\eta + J/\psi \rightarrow \bar{D}^* + D$ ($\eta + J/\psi \rightarrow \bar{D}^* + D^*$) is more than 1.8 times the one of $\pi + J/\psi \rightarrow \bar{D}^* + D$ ($\pi + J/\psi \rightarrow \bar{D}^* + D^*$). In the η -charmonium dissociation reactions the $s\bar{s}$ component of the η meson leads to the production of $D_s^{*-} + D_s^+$, $D_s^- + D_s^{*+}$ or $D_s^{*-} + D_s^{*+}$. These charmed strange mesons are not produced in the π -charmonium dissociation reactions. Based on the estimate of the η -charmonium and π -charmonium dissociation cross sections, in the following we evaluate the difference between the dissociation rates of charmonium with π and η in hadronic matter.

In hadronic matter the π and η mesons satisfy the Bose-Einstein distribution

$$f_{q\bar{q}}(\vec{k}) = \frac{1}{e^{\sqrt{m_{q\bar{q}}^2 + \vec{k}^2}/T} - 1}, \quad (13)$$

where $m_{q\bar{q}}$ is the $q\bar{q}$ mass. The $q\bar{q}$ number density is

$$n_{q\bar{q}} = g_{q\bar{q}} \int \frac{d^3k}{(2\pi)^3} f_{q\bar{q}}(\vec{k}), \quad (14)$$

where $g_{q\bar{q}}$ is the spin-isospin degeneracy factor and equals 3 for the pion and 1 for the η meson. The thermal-averaged meson-charmonium dissociation cross section is

$$\langle v_{\text{rel}} \sigma^{\text{unpol}}(\sqrt{s}, T) \rangle = \frac{g_{q\bar{q}} \int \frac{d^3k}{(2\pi)^3} v_{\text{rel}} \sigma^{\text{unpol}}(\sqrt{s}, T) f_{q\bar{q}}(\vec{k})}{g_{q\bar{q}} \int \frac{d^3k}{(2\pi)^3} f_{q\bar{q}}(\vec{k})}, \quad (15)$$

where v_{rel} is the relative velocity of the $q\bar{q}$ meson and the charmonium. The dissociation rate of the charmonium in the interaction with the $q\bar{q}$ meson in hadronic matter is

$$n_{q\bar{q}} \langle v_{\text{rel}} \sigma^{\text{unpol}}(\sqrt{s}, T) \rangle, \quad (16)$$

which determines charmonium suppression in mesonic matter [33]. The larger the dissociation rate is, the stronger suppression this mesonic matter causes. The ratio of the dissociation rates of charmonium in the interactions with η and π is

$$R_{\eta/\pi} = \frac{n_{\eta} \langle v_{\text{rel}} \sigma_{\eta c\bar{c}}^{\text{unpol}}(\sqrt{s}, T) \rangle}{n_{\pi} \langle v_{\text{rel}} \sigma_{\pi c\bar{c}}^{\text{unpol}}(\sqrt{s}, T) \rangle}, \quad (17)$$

where n_{η} and n_{π} are the number densities of η and π mesons, respectively; $\sigma_{\eta c\bar{c}}^{\text{unpol}}$ and $\sigma_{\pi c\bar{c}}^{\text{unpol}}$ are the unpolarised cross sections for a η -charmonium dissociation reaction and a π -charmonium dissociation reaction, respectively. We calculate the ratio for the six sets of reactions:

- (1) $\eta + J/\psi \rightarrow \bar{D}^* + D, \quad \pi + J/\psi \rightarrow \bar{D}^* + D;$
- (2) $\eta + J/\psi \rightarrow \bar{D}^* + D^*, \quad \pi + J/\psi \rightarrow \bar{D}^* + D^*;$
- (3) $\eta + \psi' \rightarrow \bar{D}^* + D, \quad \pi + \psi' \rightarrow \bar{D}^* + D;$
- (4) $\eta + \psi' \rightarrow \bar{D}^* + D^*, \quad \pi + \psi' \rightarrow \bar{D}^* + D^*;$
- (5) $\eta + \chi_c \rightarrow \bar{D}^* + D, \quad \pi + \chi_c \rightarrow \bar{D}^* + D;$
- (6) $\eta + \chi_c \rightarrow \bar{D}^* + D^*, \quad \pi + \chi_c \rightarrow \bar{D}^* + D^*.$

Results are shown in Figs. 24-29. The two reactions in each set have the same final states. The ratio decreases with charmonium momentum increase. For $\eta + \psi' \rightarrow \bar{D}^* + D$ and $\pi + \psi' \rightarrow \bar{D}^* + D$ the ratio in Fig. 26 is smaller than 0.018. For $\eta + \psi' \rightarrow \bar{D}^* + D^*$ and $\pi + \psi' \rightarrow \bar{D}^* + D^*$ the ratio in Fig. 27 is smaller than 0.82. For $\eta + \chi_c \rightarrow \bar{D}^* + D$ and

$\pi + \chi_c \rightarrow \bar{D}^* + D$ the ratio in Fig. 28 is smaller than 0.08. For $\eta + \chi_c \rightarrow \bar{D}^* + D^*$ and $\pi + \chi_c \rightarrow \bar{D}^* + D^*$ the ratio in Fig. 29 is smaller than 0.72. For $\eta + J/\psi \rightarrow \bar{D}^* + D$ and $\pi + J/\psi \rightarrow \bar{D}^* + D$ the ratio at $T/T_c=0.65, 0.75, 0.9$ and 0.95 in Fig. 24 is smaller than 0.73 and the ratio at $T/T_c=0.85$ is larger than 1 when the J/ψ momentum is smaller than 0.7 GeV/c. For $\eta + J/\psi \rightarrow \bar{D}^* + D^*$ and $\pi + J/\psi \rightarrow \bar{D}^* + D^*$ the ratio at $T/T_c=0.65$ and 0.95 in Fig. 25 is smaller than 0.51 and the ratio at $T/T_c=0.75, 0.85$ and 0.9 is larger than 1 when the J/ψ momentum is smaller than 0.6 GeV/c, 3.3 GeV/c and 6.6 GeV/c, respectively. Therefore, compared to the dissociation rate of ψ' (χ_c) with π , the dissociation rate of ψ' (χ_c) with η may be neglected; but the dissociation rate of J/ψ with η is comparable to the dissociation rate of J/ψ with π at low J/ψ momenta. To study the J/ψ suppression in hadronic matter, the $\eta + J/\psi$ dissociation reactions need to be considered.

4 Summary

We have studied the production of $\bar{D}^*D_s^+, \bar{D}D_s^{*+}$ and $\bar{D}^*D_s^{*+}$ in the K -charmonium dissociation and the production of $\bar{D}^*D, \bar{D}D^*, \bar{D}^*D^*, D_s^{*-}D_s^+, D_s^-D_s^{*+}$ and $D_s^{*-}D_s^{*+}$ in the η -charmonium dissociation. The K -charmonium dissociation includes 9 reactions and the η -charmonium dissociation includes 18 reactions. The cross sections for the 27 reactions are calculated with the temperature-dependent quark potential, in the Born approximation and in the quark-interchange mechanism. The cross sections for the \bar{K} -charmonium dissociation reactions are identical to the cross sections for the K -charmonium dissociation reactions. The numerical cross sections are parametrized as functions of \sqrt{s} . The temperature dependence of the peak cross sections of the endothermic K -charmonium dissociation reactions is closely related to the temperature dependence of the K radius, the charmonia radii, the confinement and the node of the ψ' wave function. For $0.6 \leq T/T_c < 1$ the cross sections for $\bar{D}^*D, \bar{D}D^*$ and \bar{D}^*D^* produced in the endothermic $\eta + J/\psi$ reactions around their cross-section peaks are larger than the ones for $\bar{D}^*D_s^+, \bar{D}D_s^{*+}$ and $\bar{D}^*D_s^{*+}$ produced in the endothermic $K + J/\psi$ reactions, respectively. For $0.6 \leq T/T_c < 1$ the cross sections

for the η -charmonium dissociation reactions are larger than the cross sections for the π -charmonium dissociation reactions. To the ψ' and χ_c suppression in hadronic matter the $\eta + \psi'$ and $\eta + \chi_c$ dissociation reactions may be neglected, but to the J/ψ suppression the $\eta + J/\psi$ dissociation reactions need to be taken into account.

Acknowledgements

This work was supported by the National Natural Science Foundation of China under Grant No. 11175111. We thank P. McGuire and H. J. Weber for careful readings of the manuscript.

Appendix A

The numerical cross sections for the endothermic reactions in Figs. 3-13 and 18-23 can be parametrized as

$$\begin{aligned} \sigma^{\text{unpol}}(\sqrt{s}, T) = & a_1 \left(\frac{\sqrt{s} - \sqrt{s_0}}{b_1} \right)^{c_1} \exp \left[c_1 \left(1 - \frac{\sqrt{s} - \sqrt{s_0}}{b_1} \right) \right] \\ & + a_2 \left(\frac{\sqrt{s} - \sqrt{s_0}}{b_2} \right)^{c_2} \exp \left[c_2 \left(1 - \frac{\sqrt{s} - \sqrt{s_0}}{b_2} \right) \right], \end{aligned}$$

and for the exothermic reactions in Figs. 6-10, 12-17 and 20-21

$$\begin{aligned} \sigma^{\text{unpol}}(\sqrt{s}, T) = & \frac{\vec{P}^2}{\bar{P}^2} \left\{ a_1 \left(\frac{\sqrt{s} - \sqrt{s_0}}{b_1} \right)^{c_1} \exp \left[c_1 \left(1 - \frac{\sqrt{s} - \sqrt{s_0}}{b_1} \right) \right] \right. \\ & \left. + a_2 \left(\frac{\sqrt{s} - \sqrt{s_0}}{b_2} \right)^{c_2} \exp \left[c_2 \left(1 - \frac{\sqrt{s} - \sqrt{s_0}}{b_2} \right) \right] \right\}, \end{aligned}$$

with

$$\begin{aligned} \vec{P}^2(\sqrt{s}) &= \frac{1}{4s} \left\{ [s - (m_{q\bar{q}}^2 + m_{c\bar{c}}^2)]^2 - 4m_{q\bar{q}}^2 m_{c\bar{c}}^2 \right\}, \\ \bar{P}^2(\sqrt{s}) &= \frac{1}{4s} \left\{ [s - (m_{q\bar{c}}^2 + m_{c\bar{q}}^2)]^2 - 4m_{q\bar{c}}^2 m_{c\bar{q}}^2 \right\}. \end{aligned}$$

Here a_1 , b_1 , c_1 , a_2 , b_2 and c_2 are parameters and $\sqrt{s_0}$ is the threshold energy. The parameter values are listed in Tables 1-6. We also list d_0 what is the separation between the peak's location on the \sqrt{s} -axis and the threshold energy and $\sqrt{s_z}$ which is the square root of the Mandelstam variable at which the cross section is 1/100 of the peak cross section. According to a procedure presented in Ref. [18] we can get cross sections at any temperature from the quantities listed in Tables 1-6.

References

- [1] D. Kharzeev, H. Satz, Phys. Lett. B 334, 155 (1994).
- [2] M.E. Peskin, Nucl. Phys. B 156, 365 (1979); G. Bhanot, M.E. Peskin, Nucl. Phys. B 156, 391 (1979).
- [3] X.-M. Xu, D. Kharzeev, H. Satz, X.-N. Wang, Phys. Rev. C 53, 3051 (1996).
- [4] F. Arleo, P.B. Gossiaux, T. Gousset, J. Aichelin, Phys. Rev. D 65, 014005 (2001).
- [5] K. Martins, D. Blaschke, E. Quack, Phys. Rev. C 51, 2723 (1995).
- [6] I. Bender, H.G. Dosch, H.J. Pirner, H.G. Kruse, Nucl. Phys. A 414, 359 (1984).
- [7] T. Barnes, E.S. Swanson, Phys. Rev. D 46, 131 (1992); E.S. Swanson, Ann. Phys. (N.Y.) 220, 73 (1992).
- [8] C.-Y. Wong, E.S. Swanson, T. Barnes, Phys. Rev. C 62, 045201 (2000); Phys. Rev. C 65, 014903 (2001).
- [9] T. Barnes, E.S. Swanson, C.-Y. Wong, X.-M. Xu, Phys. Rev. C 68, 014903 (2003).
- [10] S.G. Matinyan, B. Müller, Phys. Rev. C 58, 2994 (1998).
- [11] Z. Lin, C.M. Ko, Phys. Rev. C 62, 034903 (2000); J. Phys. G 27, 617 (2001).
- [12] K.L. Haglin, Phys. Rev. C 61, 031902 (2000); K.L. Haglin, C. Gale, Phys. Rev. C 63, 065201 (2001).

- [13] Y. Oh, T. Song, S.H. Lee, Phys. Rev. C 63, 034901 (2001).
- [14] F.S. Navarra, M. Nielsen, M.R. Robilotta, Phys. Rev. C 64, 021901(R) (2001).
- [15] L. Maiani, F. Piccinini, A.D. Polosa, V. Riquer, Nucl. Phys. A 741, 273 (2004).
- [16] A. Bourque, C. Gale, Phys. Rev. C 78, 035206 (2008); 80, 015204 (2009).
- [17] C.-Y. Wong, Phys. Rev. C 65, 034902 (2002).
- [18] J. Zhou, X.-M. Xu, Phys. Rev. C 85, 064904 (2012).
- [19] S.S. Adler, et al., PHENIX Collaboration, Phys. Rev. C 69, 034909 (2004).
- [20] B. Abelev, et al., ALICE Collaboration, Phys. Lett. B 736, 196 (2014).
- [21] B. Sahlmüller, J. Phys. G 34, S969 (2007).
- [22] Y.-Q. Li, X.-M. Xu, Nucl. Phys. A 794, 210 (2007).
- [23] N.F. Mott, H.S.W. Massey, The Theory of Atomic Collisions, Clarendon Press, Oxford, 1965.
- [24] T. Barnes, N. Black, E.S. Swanson, Phys. Rev. C 63, 025204 (2001).
- [25] C.-Y. Wong, H.W. Crater, Phys. Rev. C 63, 044907 (2001).
- [26] W. Buchmüller, S.-H. H. Tye, Phys. Rev. D 24, 132 (1981).
- [27] F. Karsch, E. Laermann, A. Peikert, Nucl. Phys. B 605, 579 (2001).
- [28] Y.-P. Zhang, X.-M. Xu, H.-J. Ge, Nucl. Phys. A 832, 112 (2010).
- [29] A. Rothkopf, T. Hatsuda, S. Sasaki, Phys. Rev. Lett. 108, 162001 (2012).
- [30] Y. Burnier, A. Rothkopf, Phys. Rev. Lett. 111, 182003 (2013).
- [31] S. H. Lee, K. Morita, T. Song, C. M. Ko, Phys. Rev. D 89, 094015 (2014).
- [32] Z.-Y. Shen, X.-M. Xu, Chin. Phys. C 39, 074103 (2015).

- [33] X.-M. Xu, Nucl. Phys. A 697, 825 (2002).
- [34] S. Godfrey, N. Isgur, Phys. Rev. D 32, 189 (1985).
- [35] K. Nakamura, et al., Particle Data Group, J. Phys. G 37, 075021 (2010).
- [36] E. Colton, et al., Phys. Rev. D 3, 2028 (1971).
- [37] N. B. Durusoy, et al., Phys. Lett. B 45, 517 (1973).
- [38] W. Hoogland, et al., Nucl. Phys. B 126, 109 (1977).
- [39] M. J. Losty, et al., Nucl. Phys. B 69, 185 (1974).

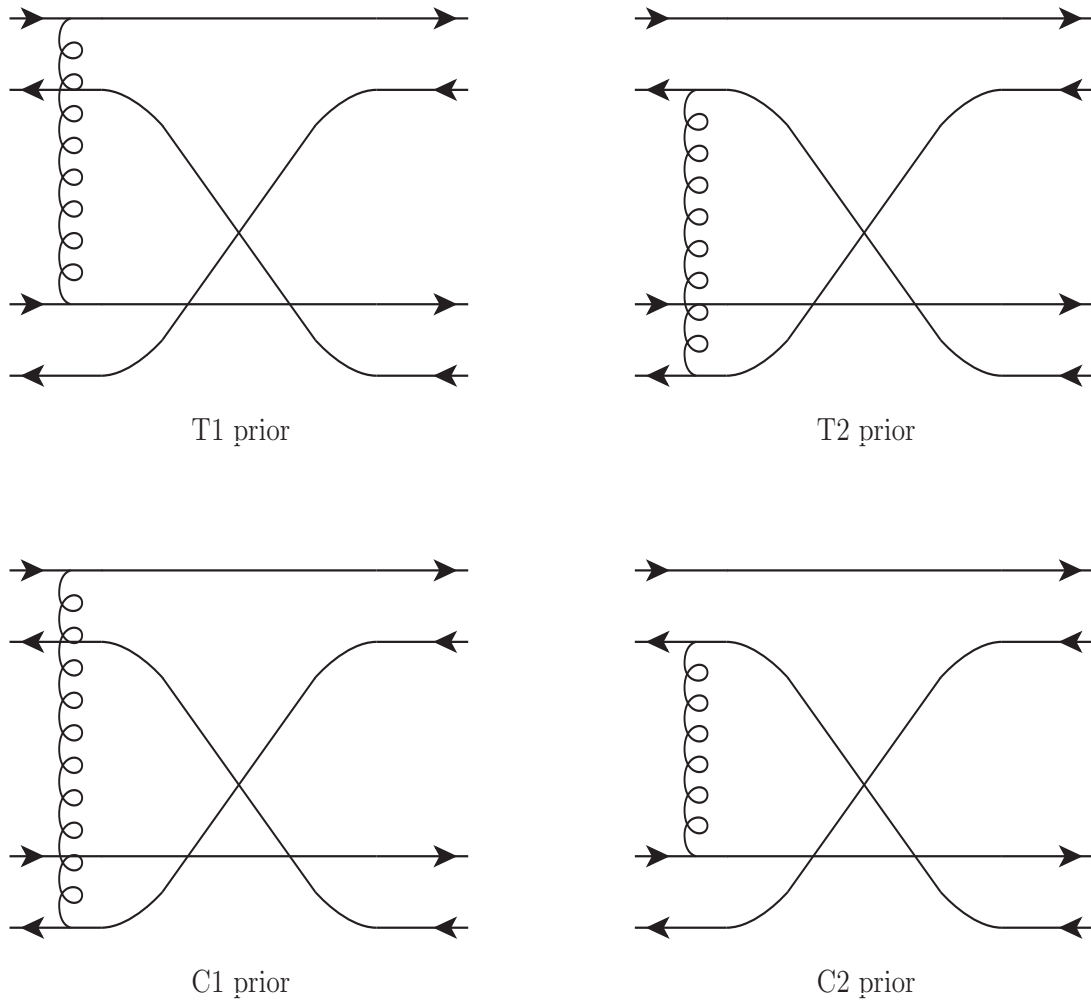


Figure 1: 'Prior' diagrams. Solid (wavy) lines represent quarks or antiquarks (gluons).

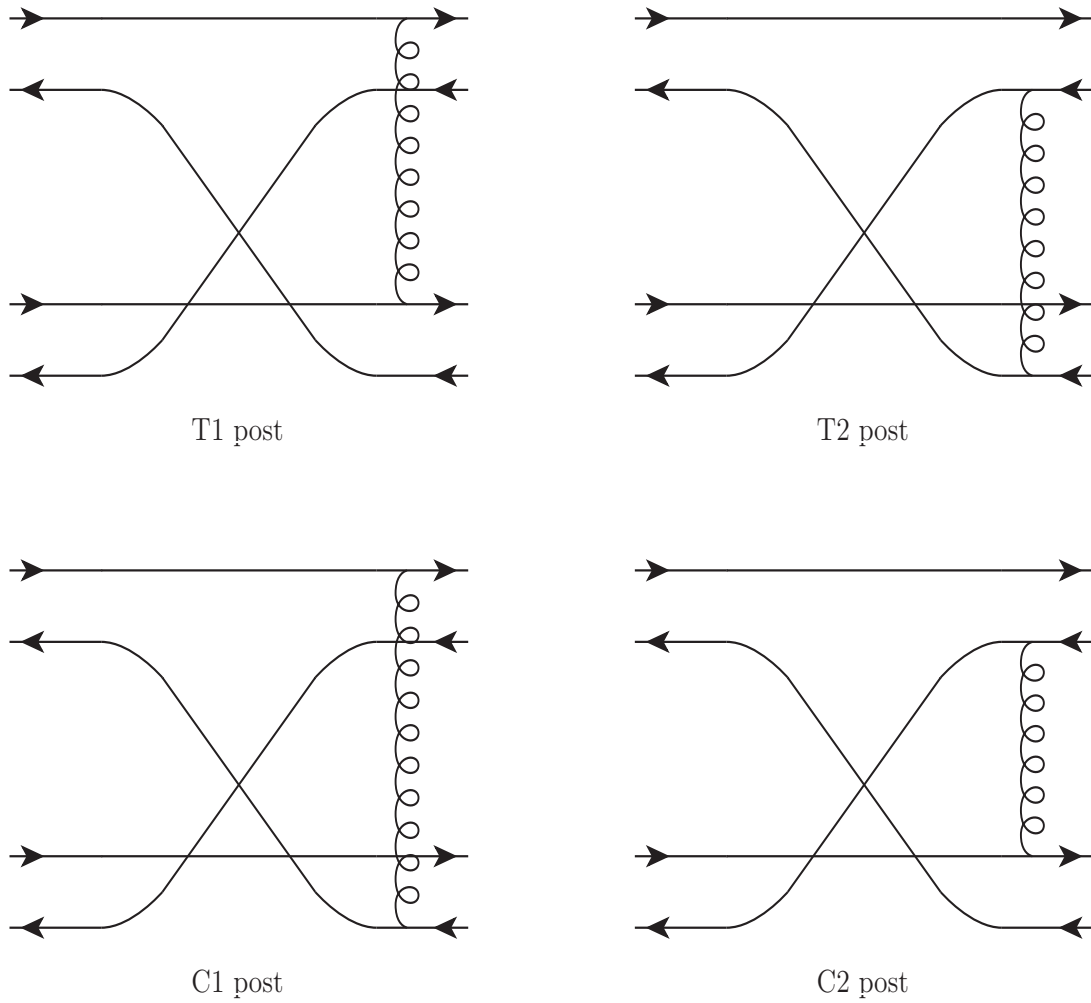


Figure 2: 'Post' diagrams. Solid (wavy) lines represent quarks or antiquarks (gluons).

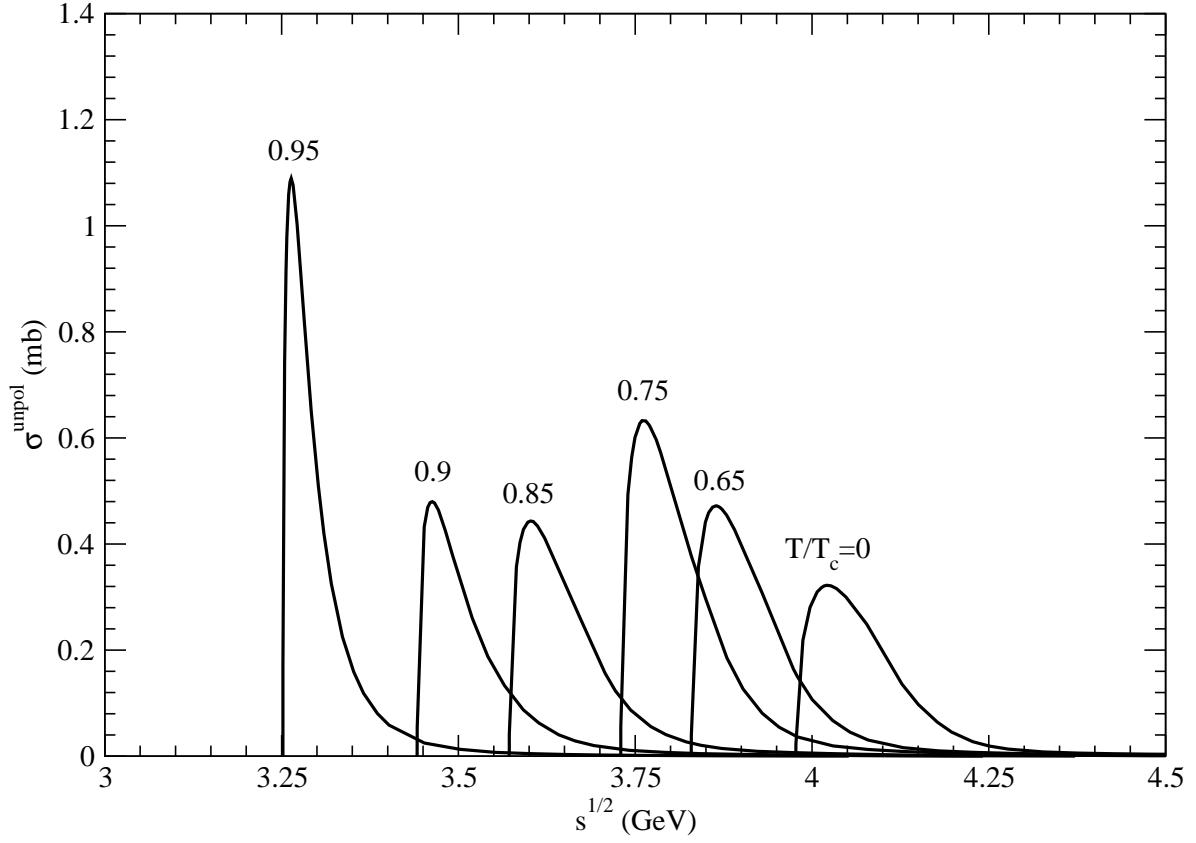


Figure 3: Cross sections for $K + J/\psi \rightarrow \bar{D}^* + D_s^+$ at various temperatures.

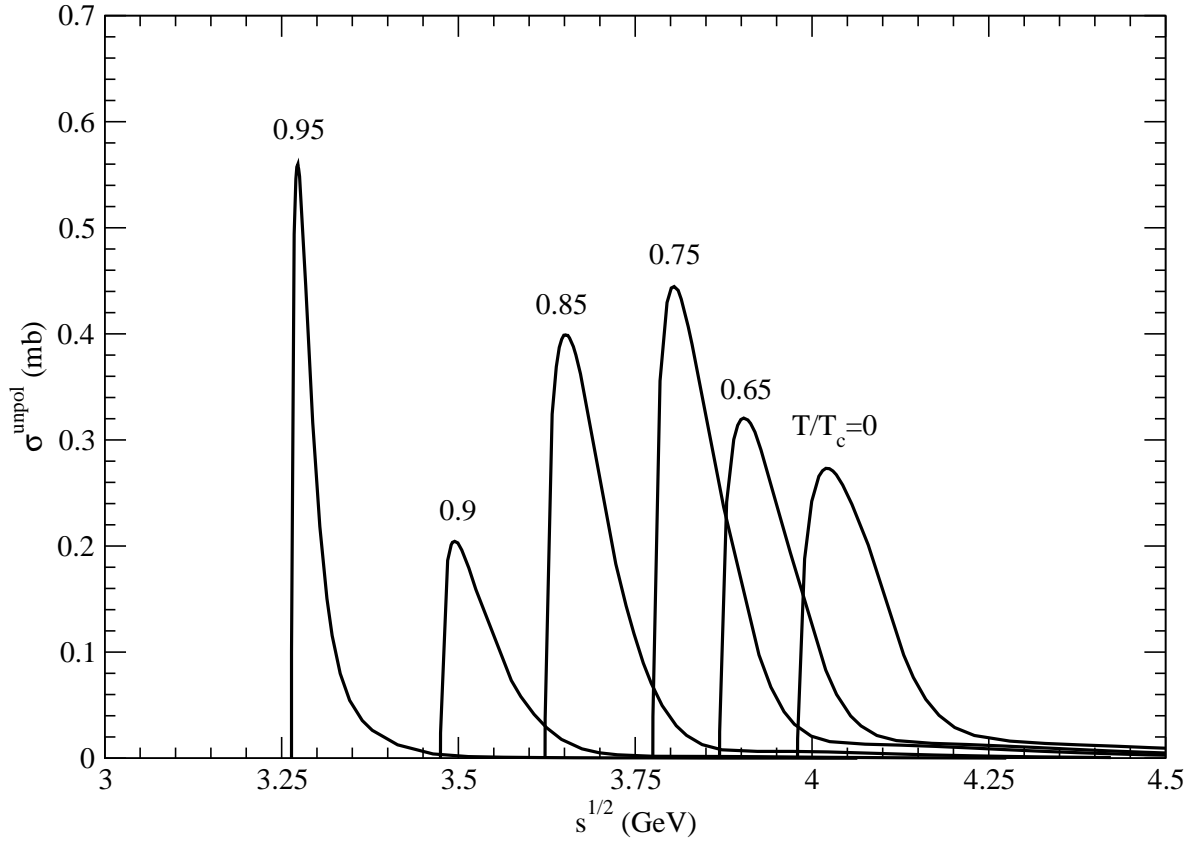


Figure 4: Cross sections for $K + J/\psi \rightarrow \bar{D} + D_s^{*+}$ at various temperatures.

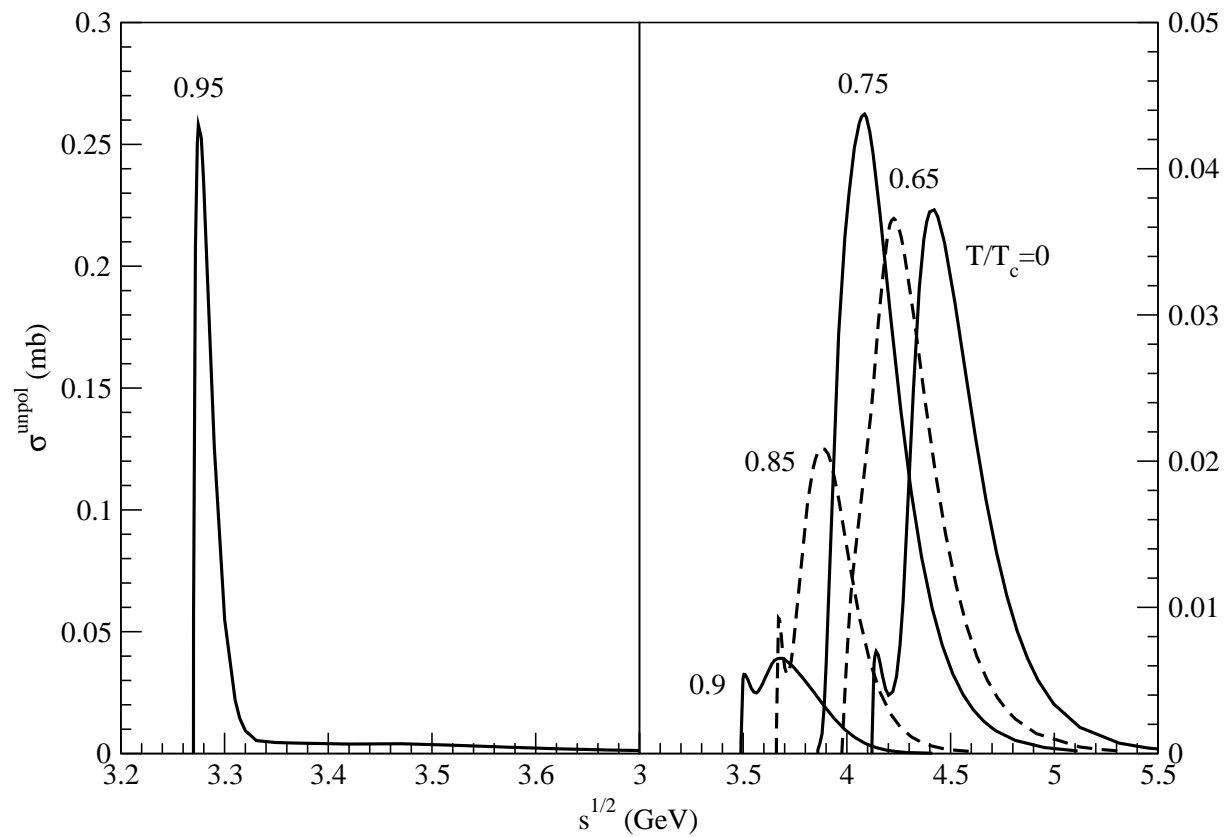


Figure 5: Cross sections for $K + J/\psi \rightarrow \bar{D}^* + D_s^{*+}$ at various temperatures.

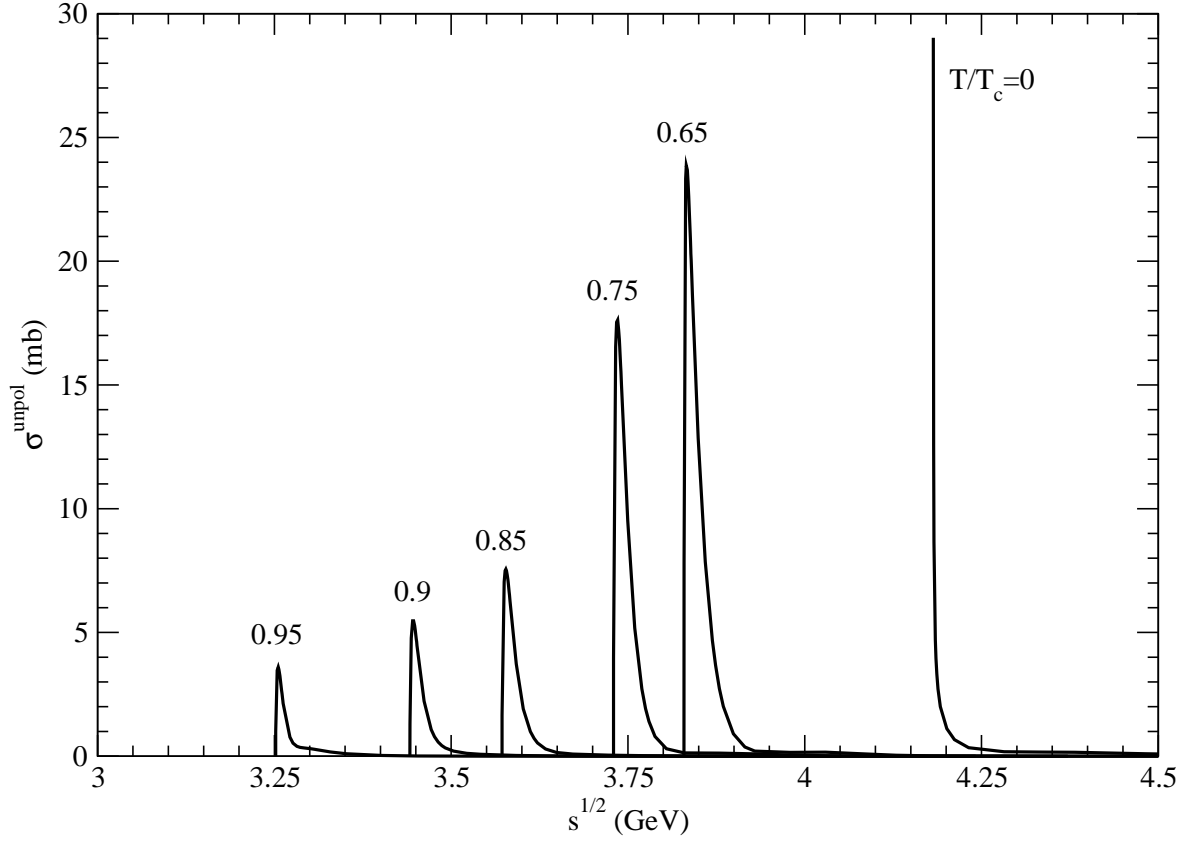


Figure 6: Cross sections for $K + \psi' \rightarrow \bar{D}^* + D_s^+$ at various temperatures.

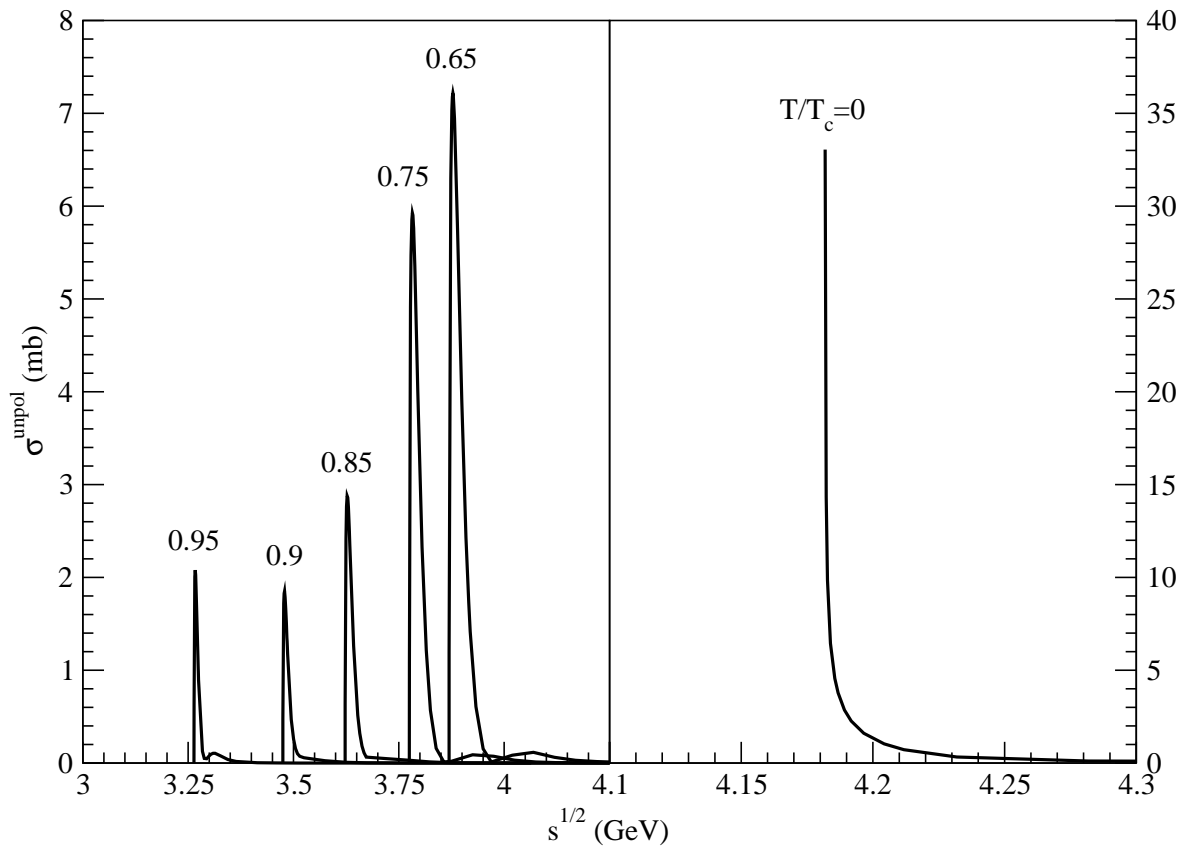


Figure 7: Cross sections for $K + \psi' \rightarrow \bar{D} + D_s^{*+}$ at various temperatures.

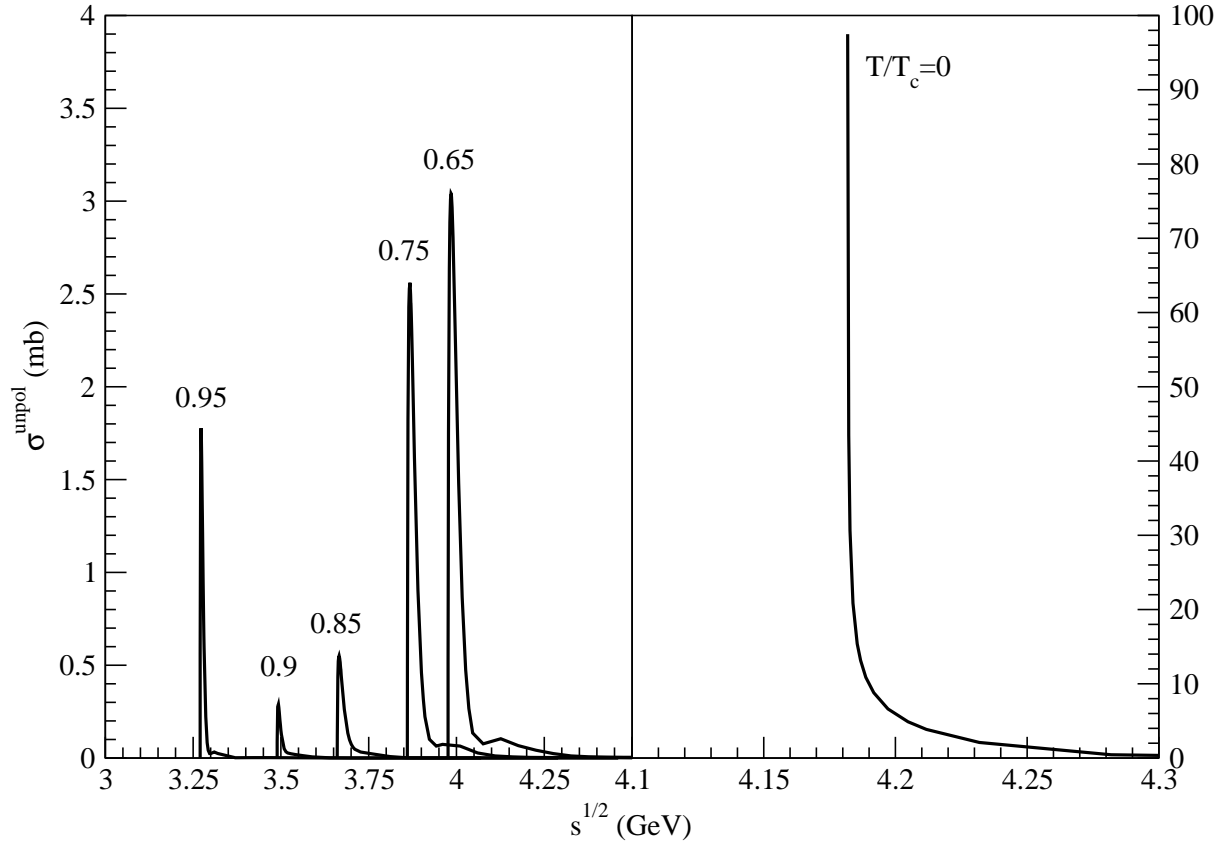


Figure 8: Cross sections for $K + \psi' \rightarrow \bar{D}^* + D_s^{*+}$ at various temperatures.

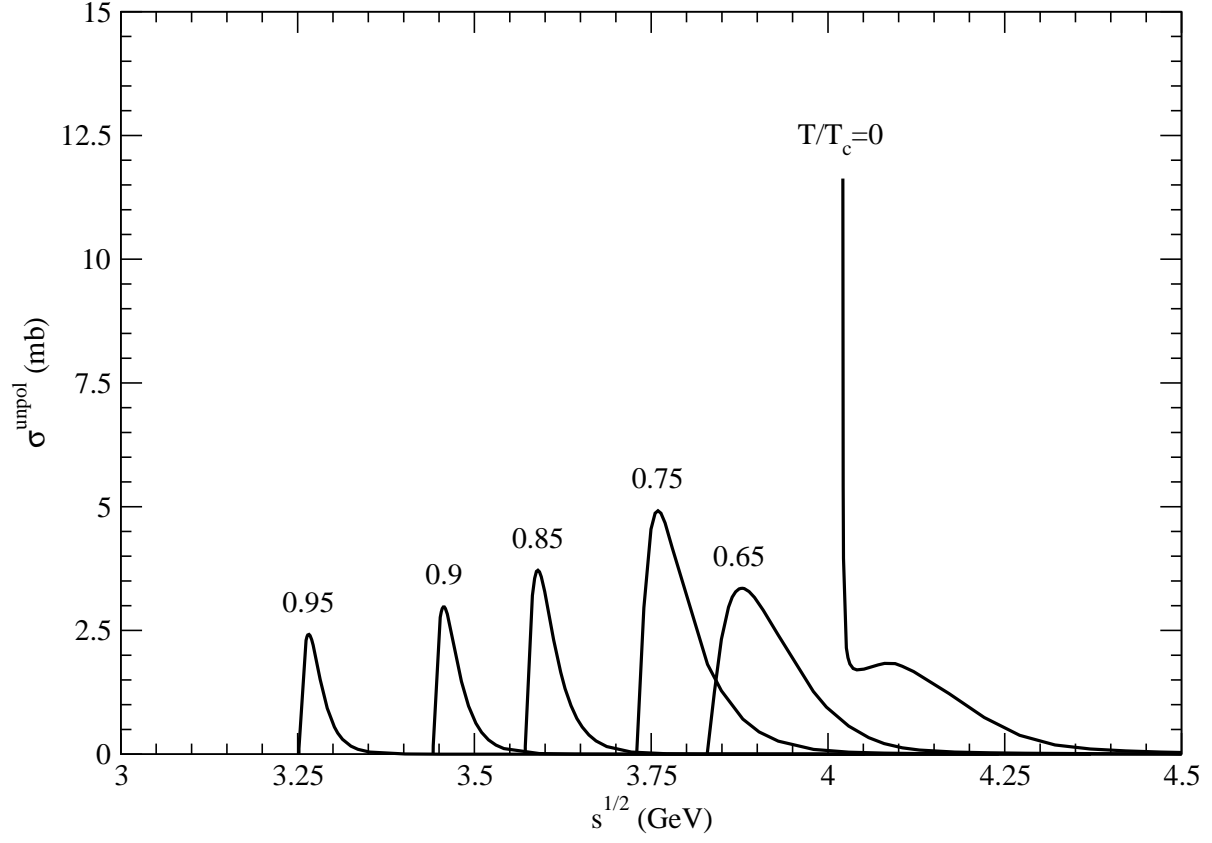


Figure 9: Cross sections for $K + \chi_c \rightarrow \bar{D}^* + D_s^+$ at various temperatures.

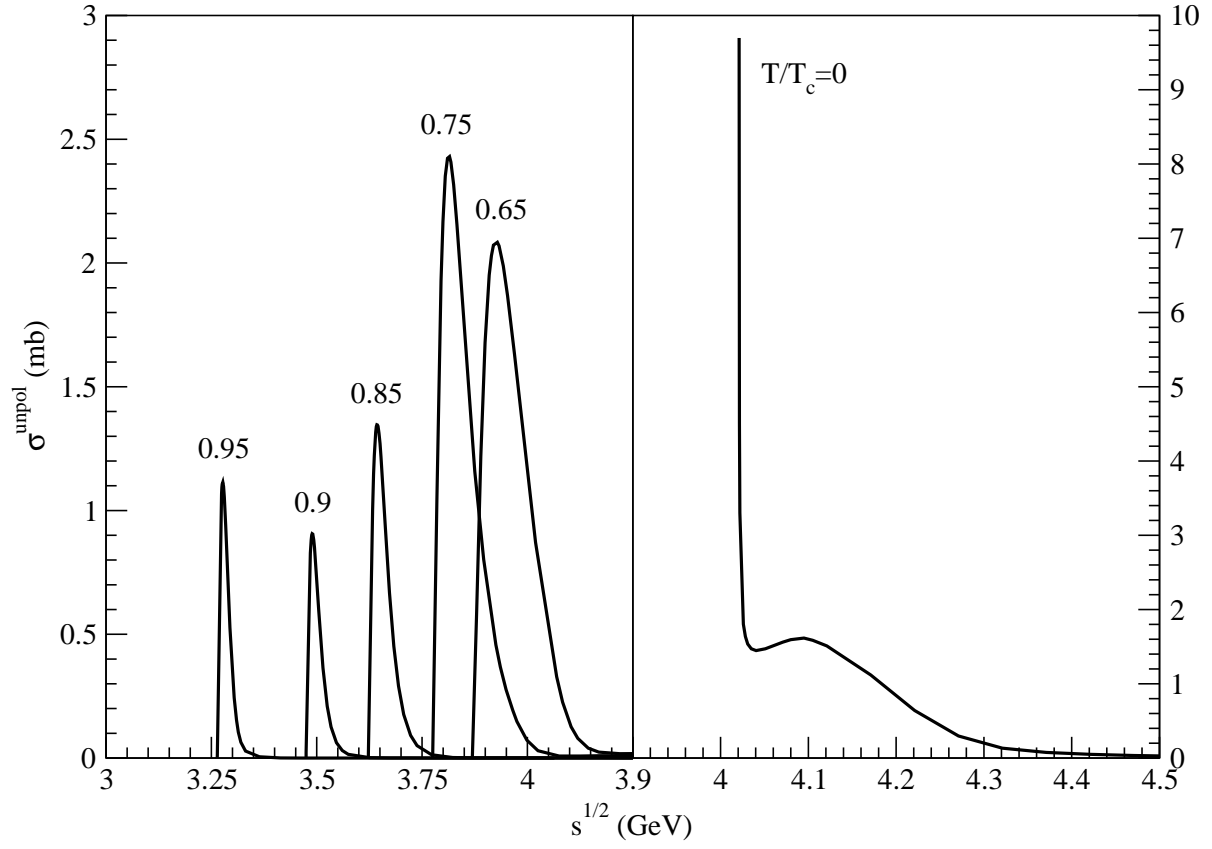


Figure 10: Cross sections for $K + \chi_c \rightarrow \bar{D} + D_s^{*+}$ at various temperatures.

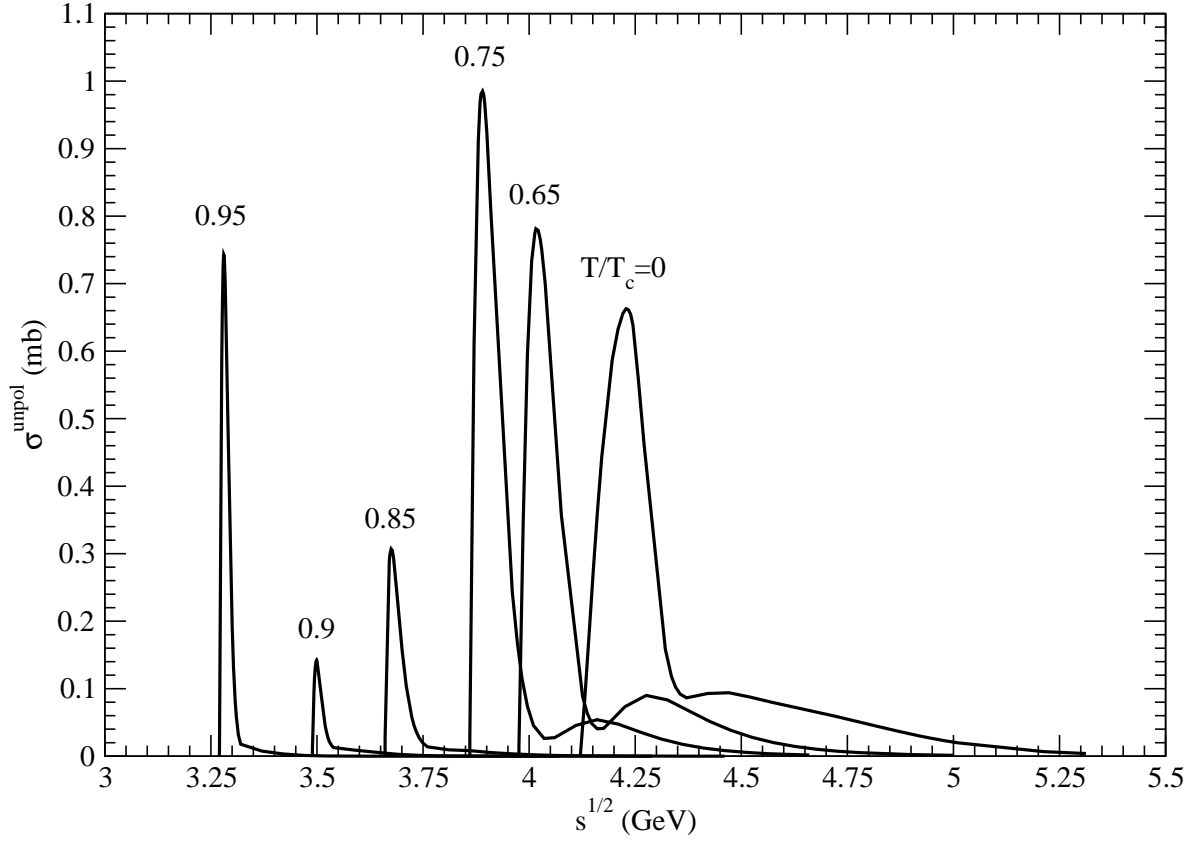


Figure 11: Cross sections for $K + \chi_c \rightarrow \bar{D}^* + D_s^{*+}$ at various temperatures.

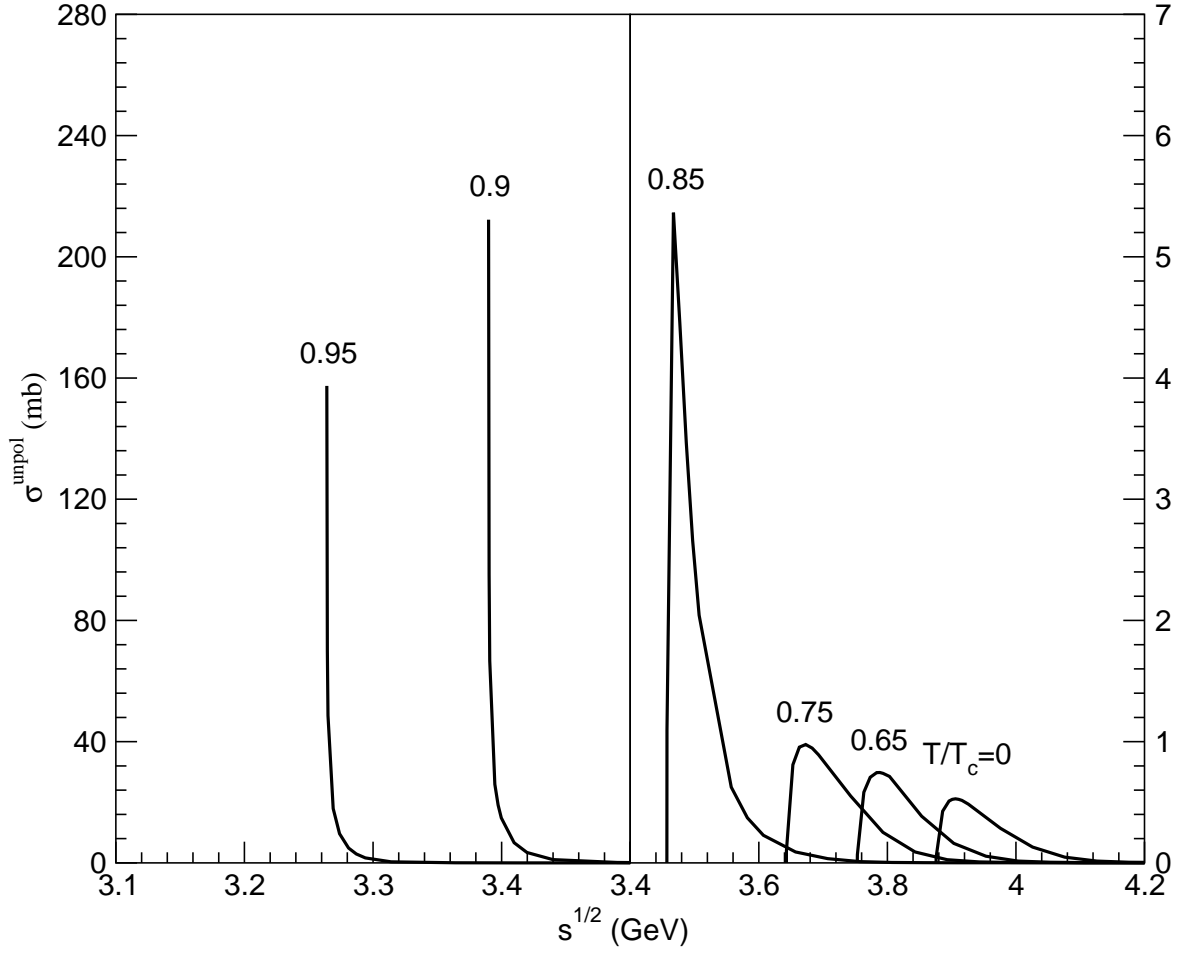


Figure 12: Cross sections for $\eta + J/\psi \rightarrow \bar{D}^* + D$ or $\bar{D} + D^*$ at various temperatures.

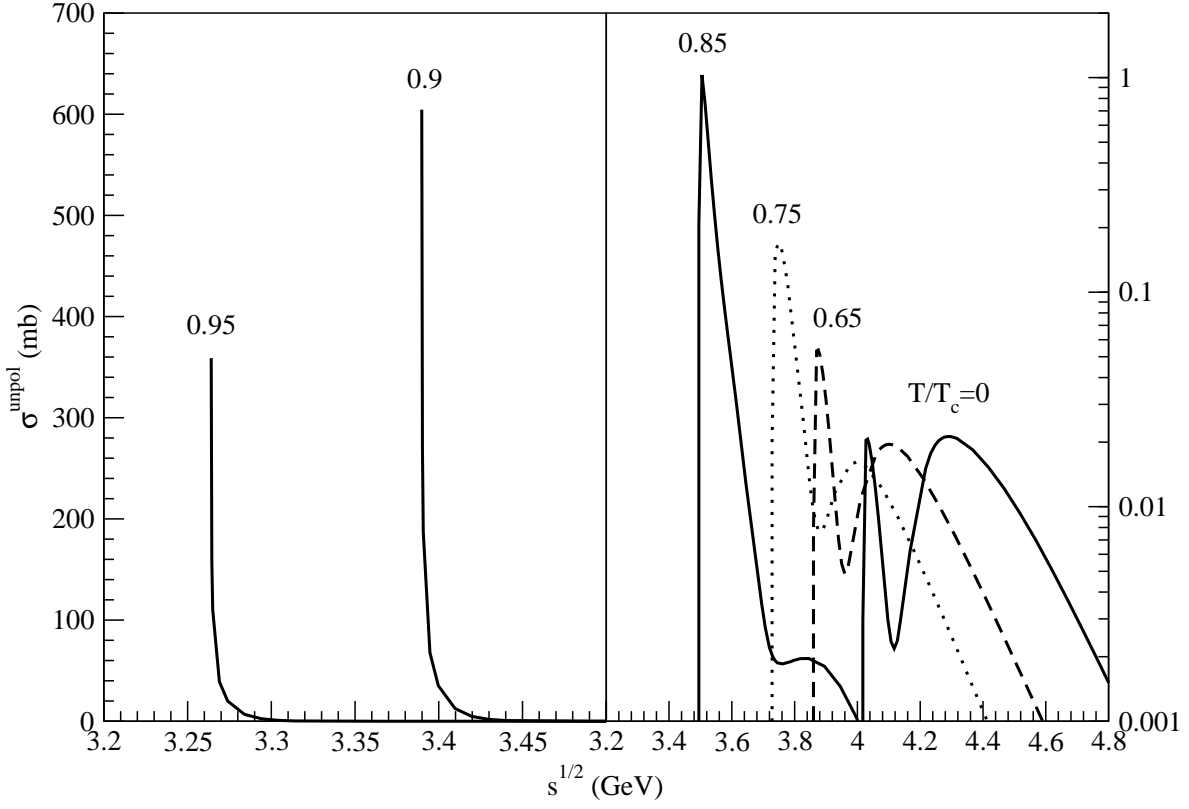


Figure 13: Cross sections for $\eta + J/\psi \rightarrow \bar{D}^* + D^*$ at various temperatures.

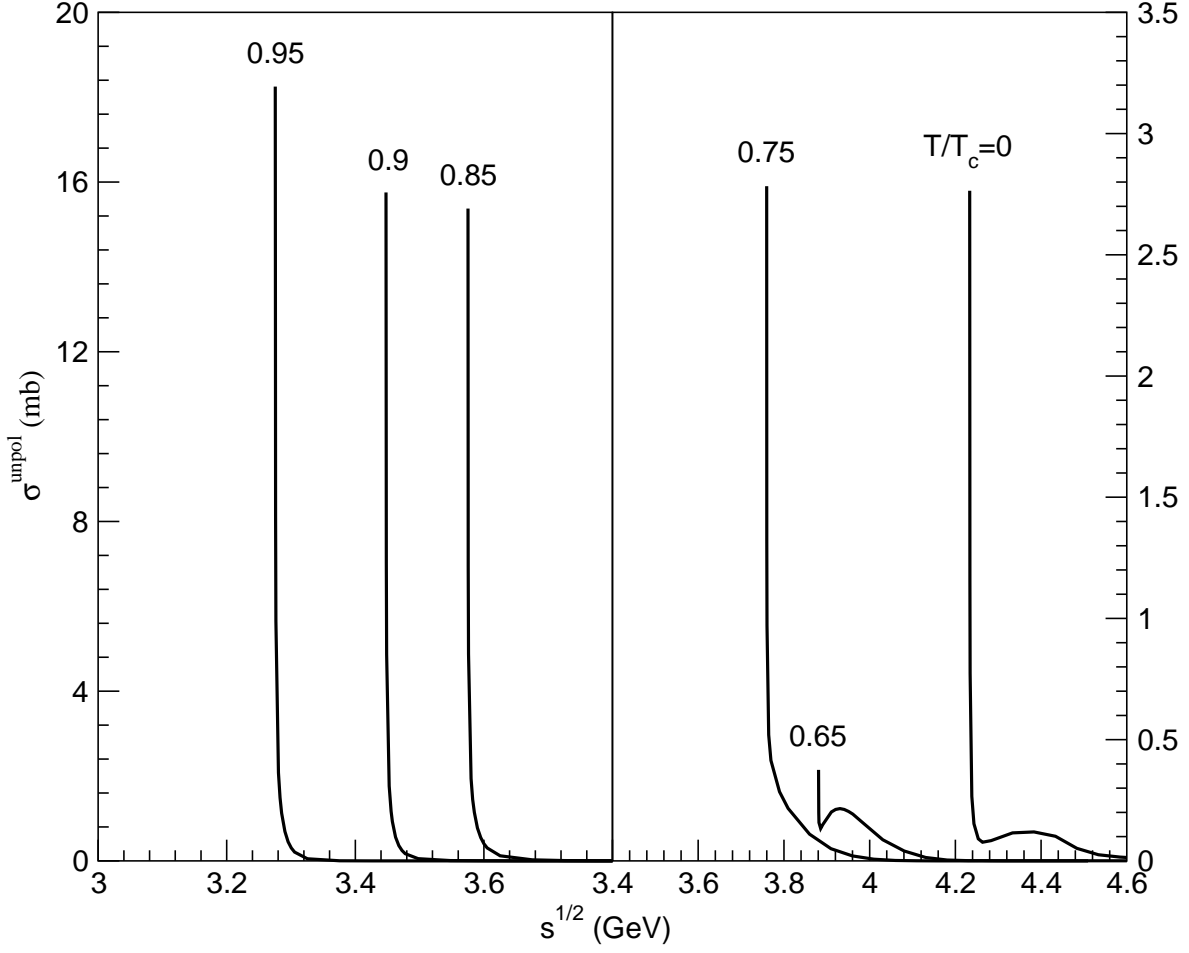


Figure 14: Cross sections for $\eta + \psi' \rightarrow \bar{D}^* + D$ or $\bar{D} + D^*$ at various temperatures.

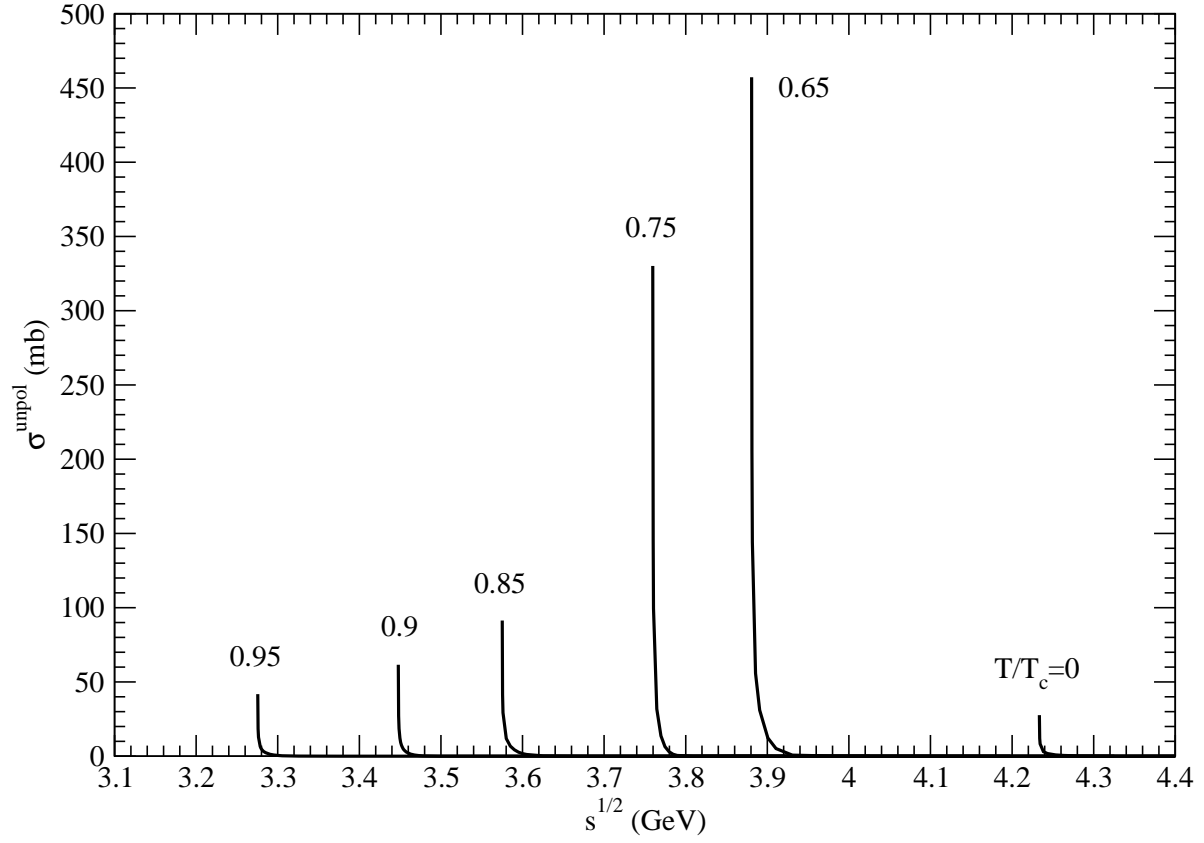


Figure 15: Cross sections for $\eta + \psi' \rightarrow \bar{D}^* + D^*$ at various temperatures.

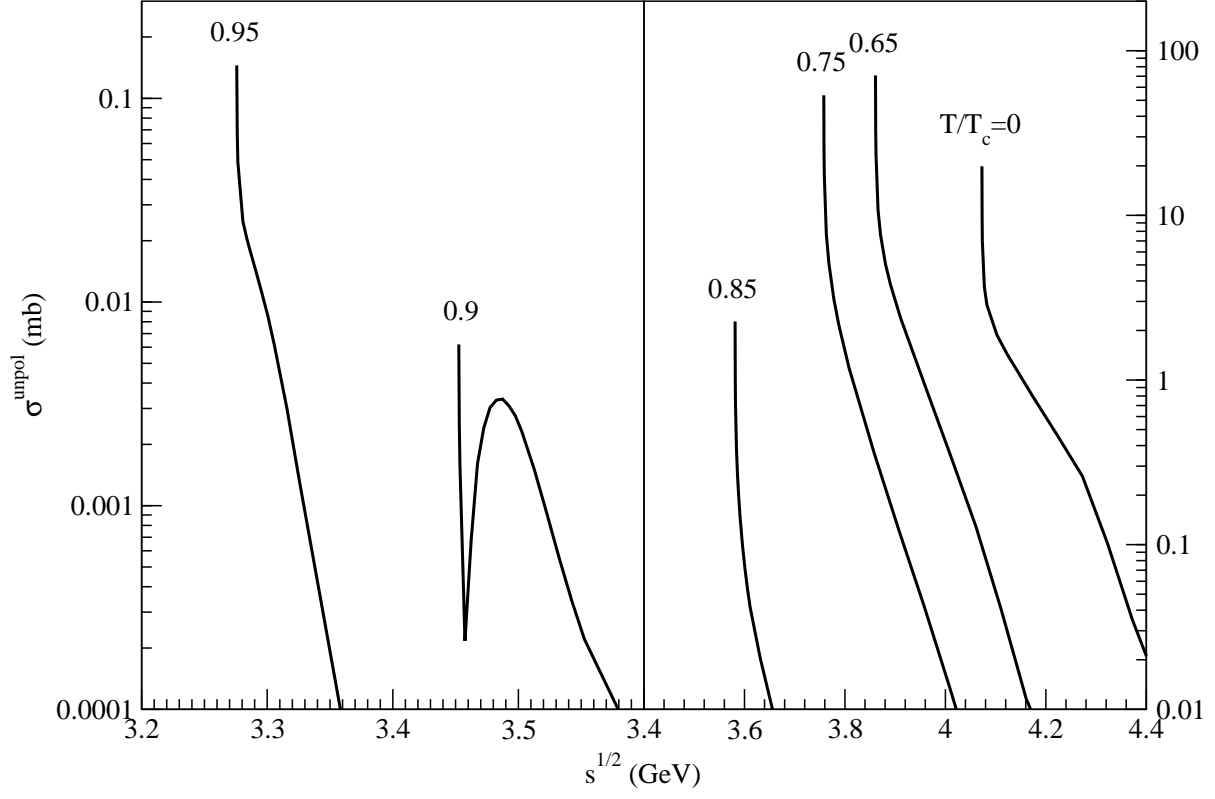


Figure 16: Cross sections for $\eta + \chi_c \rightarrow \bar{D}^* + D$ or $\bar{D} + D^*$ at various temperatures.

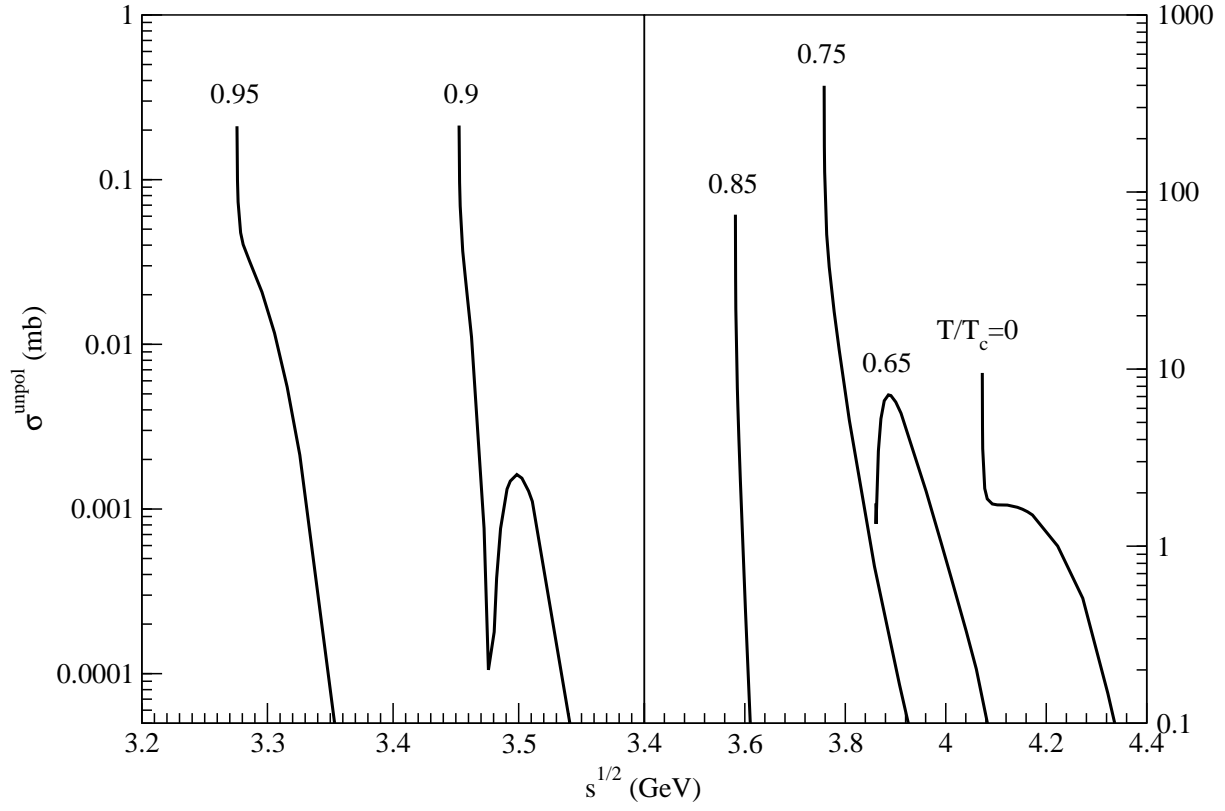


Figure 17: Cross sections for $\eta + \chi_c \rightarrow \bar{D}^* + D^*$ at various temperatures.

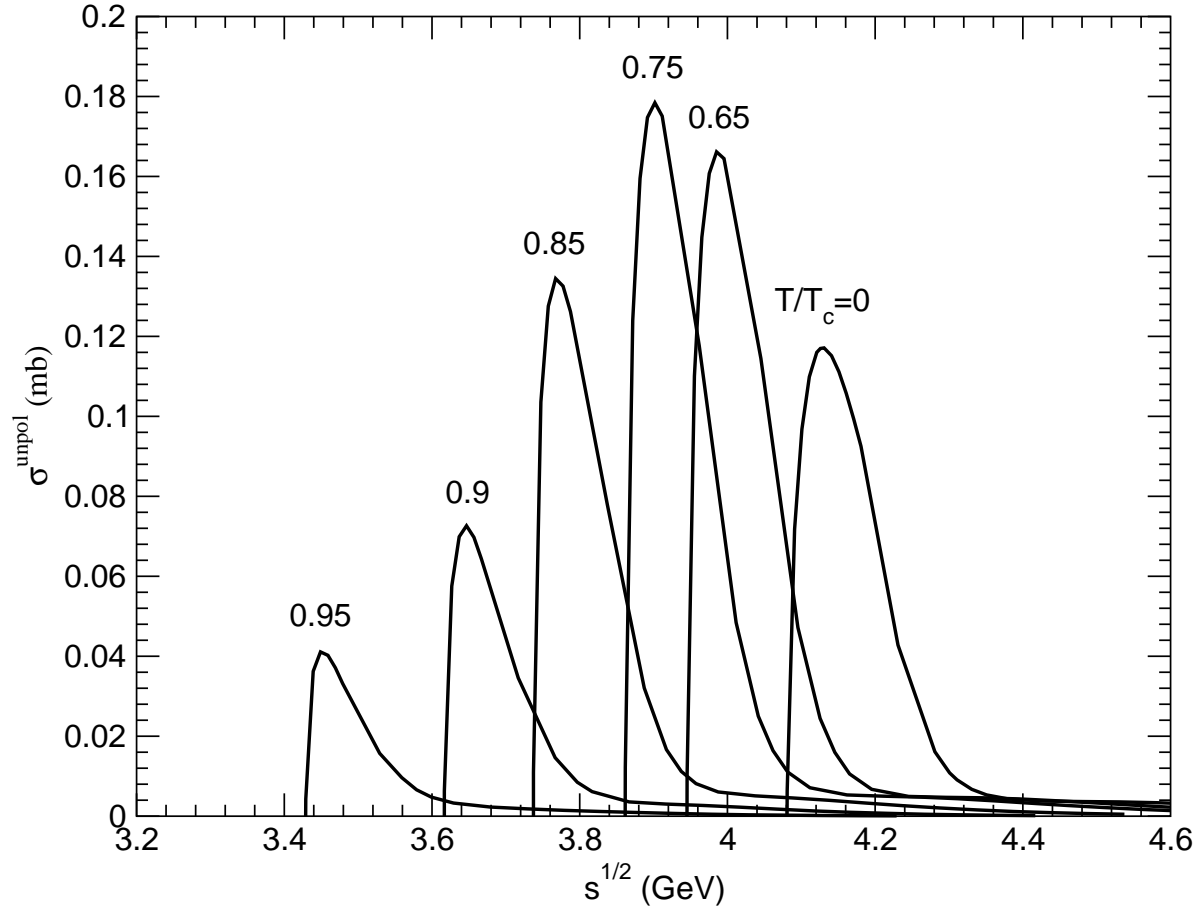


Figure 18: Cross sections for $\eta + J/\psi \rightarrow D_s^{*-} + D_s^+$ or $D_s^- + D_s^{*+}$ at various temperatures.

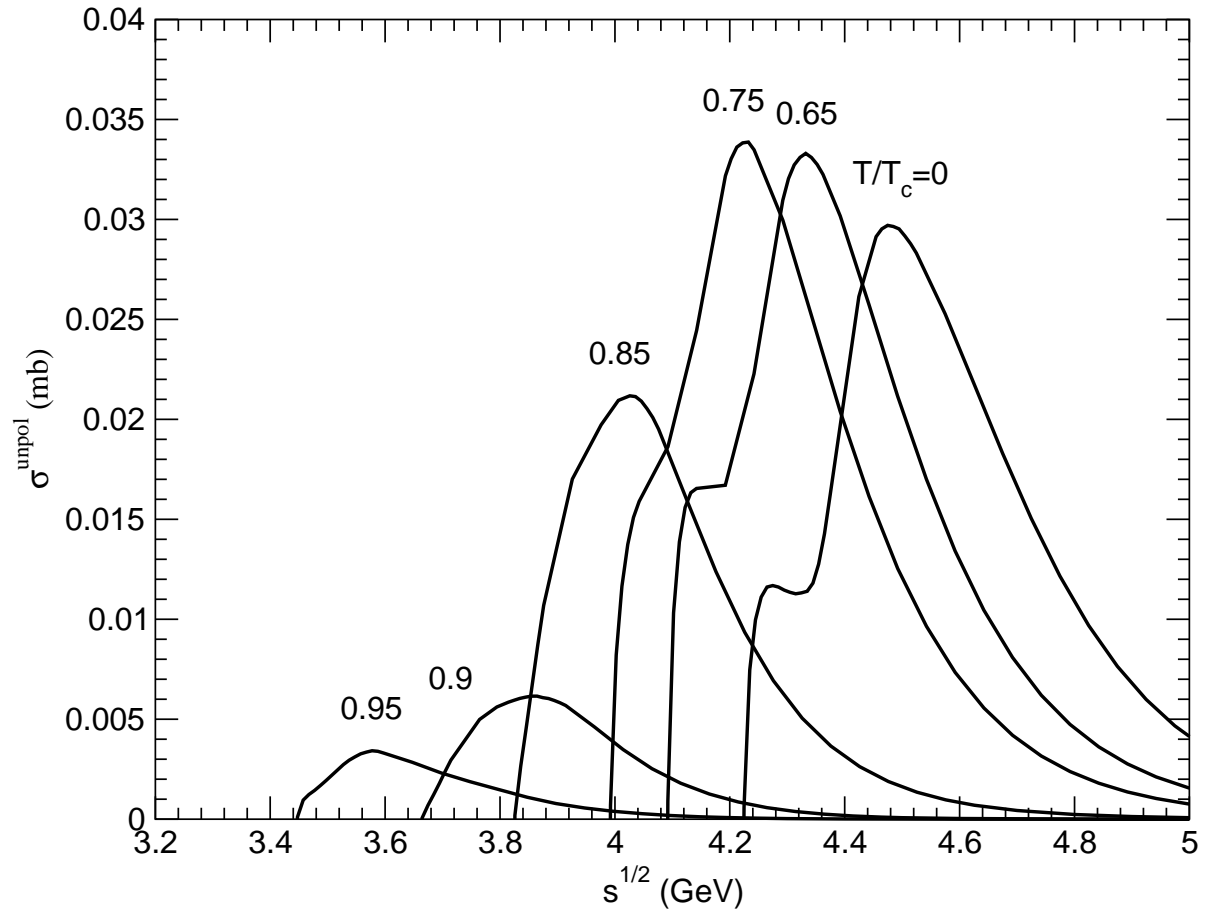


Figure 19: Cross sections for $\eta + J/\psi \rightarrow D_s^{*-} + D_s^{*+}$ at various temperatures.

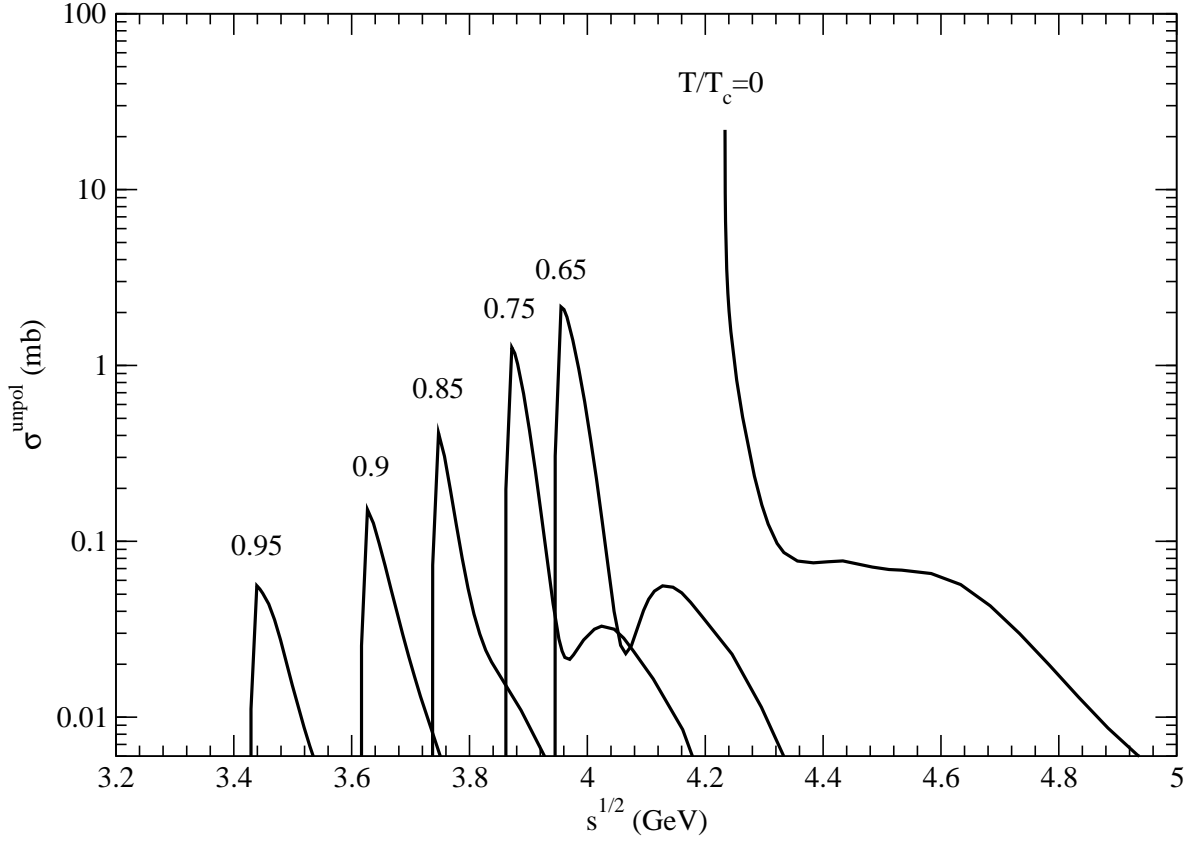


Figure 20: Cross sections for $\eta + \psi' \rightarrow D_s^{*-} + D_s^+$ or $D_s^- + D_s^{*+}$ at various temperatures.

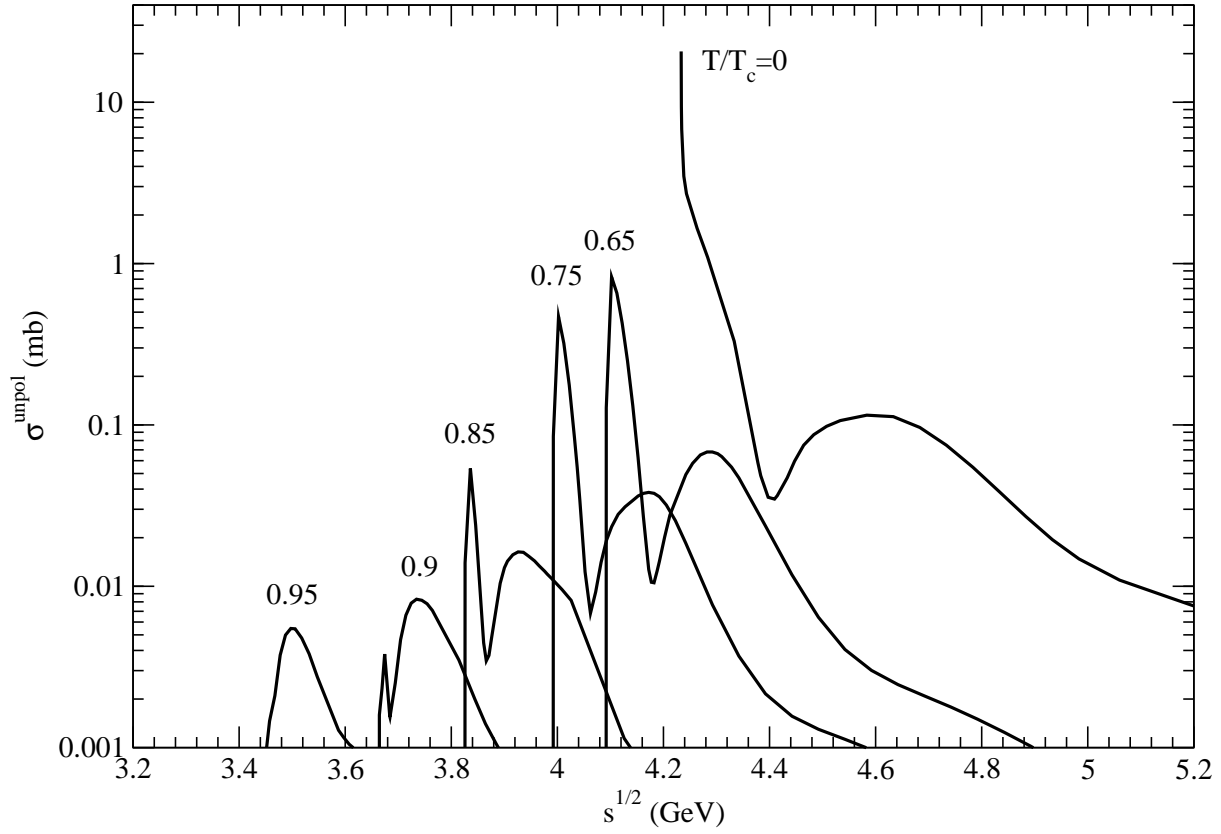


Figure 21: Cross sections for $\eta + \psi' \rightarrow D_s^{*-} + D_s^{*+}$ at various temperatures.

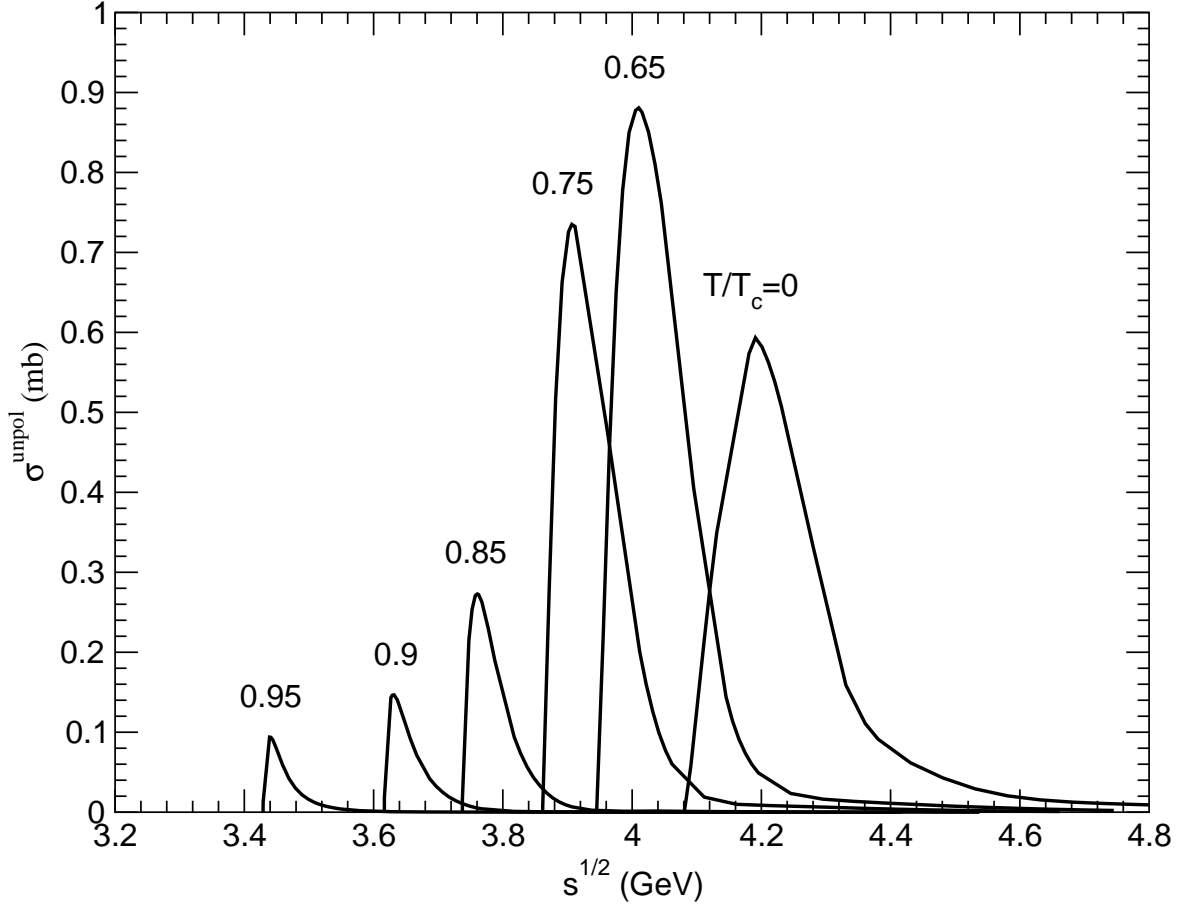


Figure 22: Cross sections for $\eta + \chi_c \rightarrow D_s^{*-} + D_s^+$ or $D_s^- + D_s^{*+}$ at various temperatures.

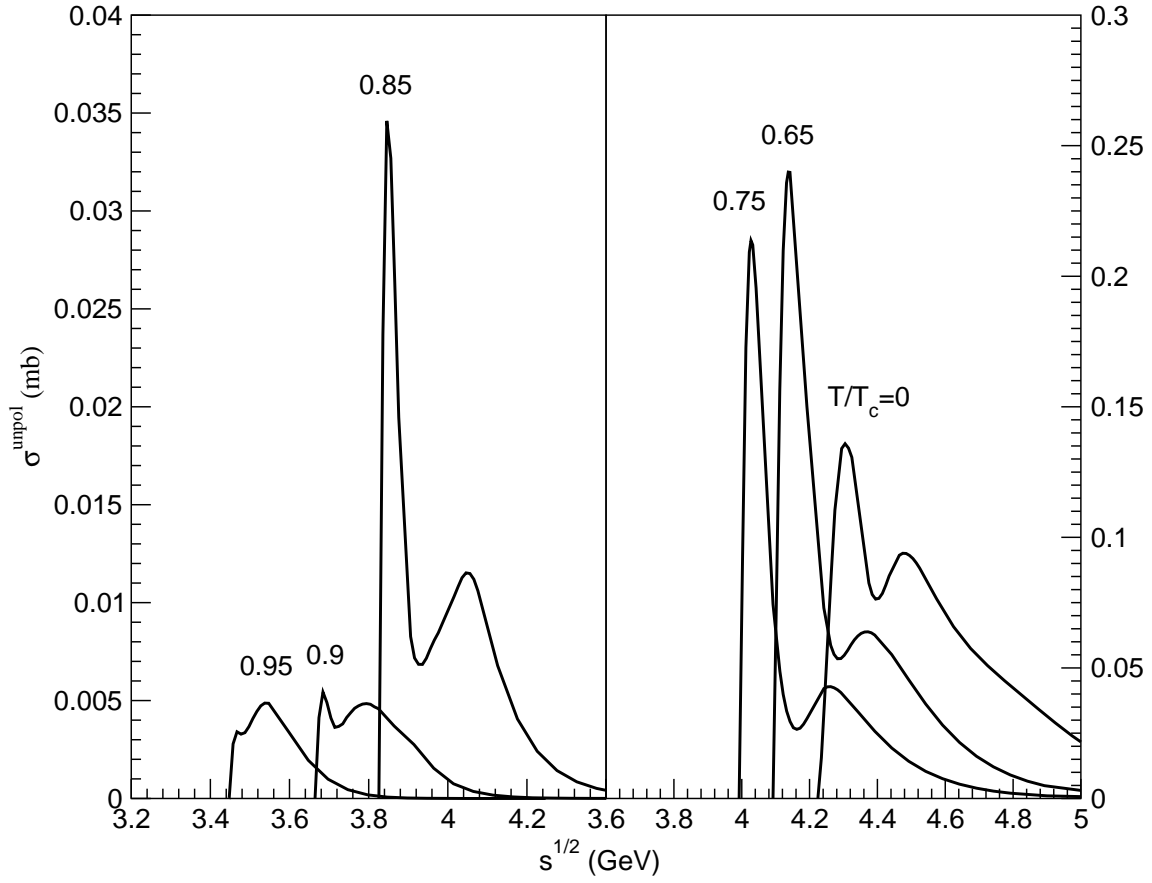


Figure 23: Cross sections for $\eta + \chi_c \rightarrow D_s^{*-} + D_s^{*+}$ at various temperatures.

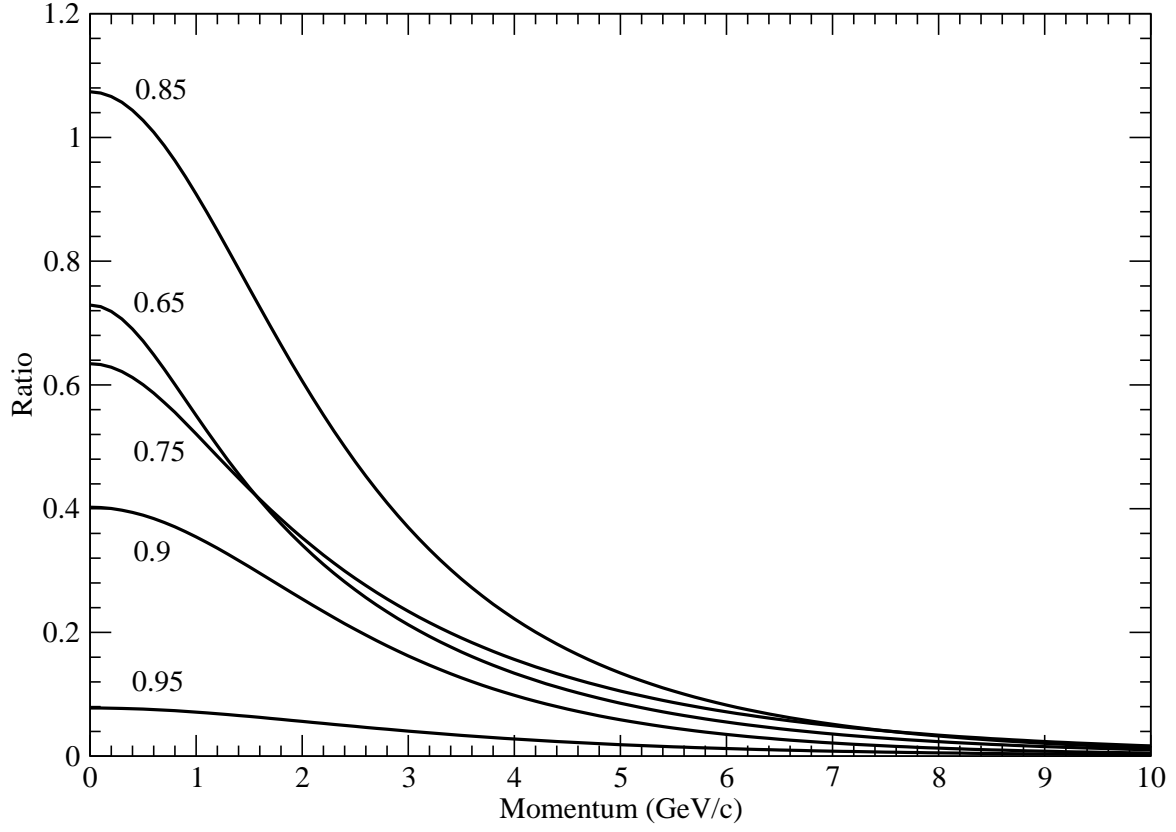


Figure 24: Ratio for $\eta + J/\psi \rightarrow \bar{D}^* + D$ and $\pi + J/\psi \rightarrow \bar{D}^* + D$ as a function of the J/ψ momentum.

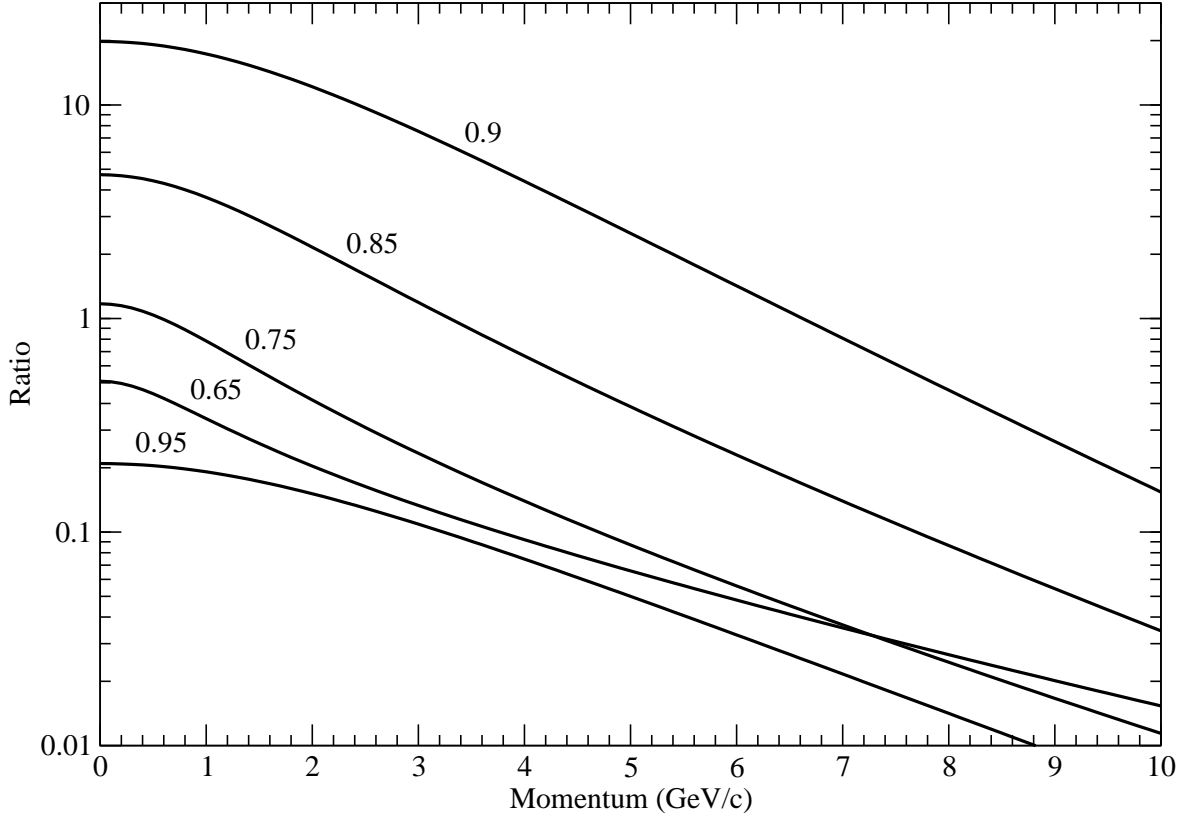


Figure 25: Ratio for $\eta + J/\psi \rightarrow \bar{D}^* + D^*$ and $\pi + J/\psi \rightarrow \bar{D}^* + D^*$ as a function of the J/ψ momentum.

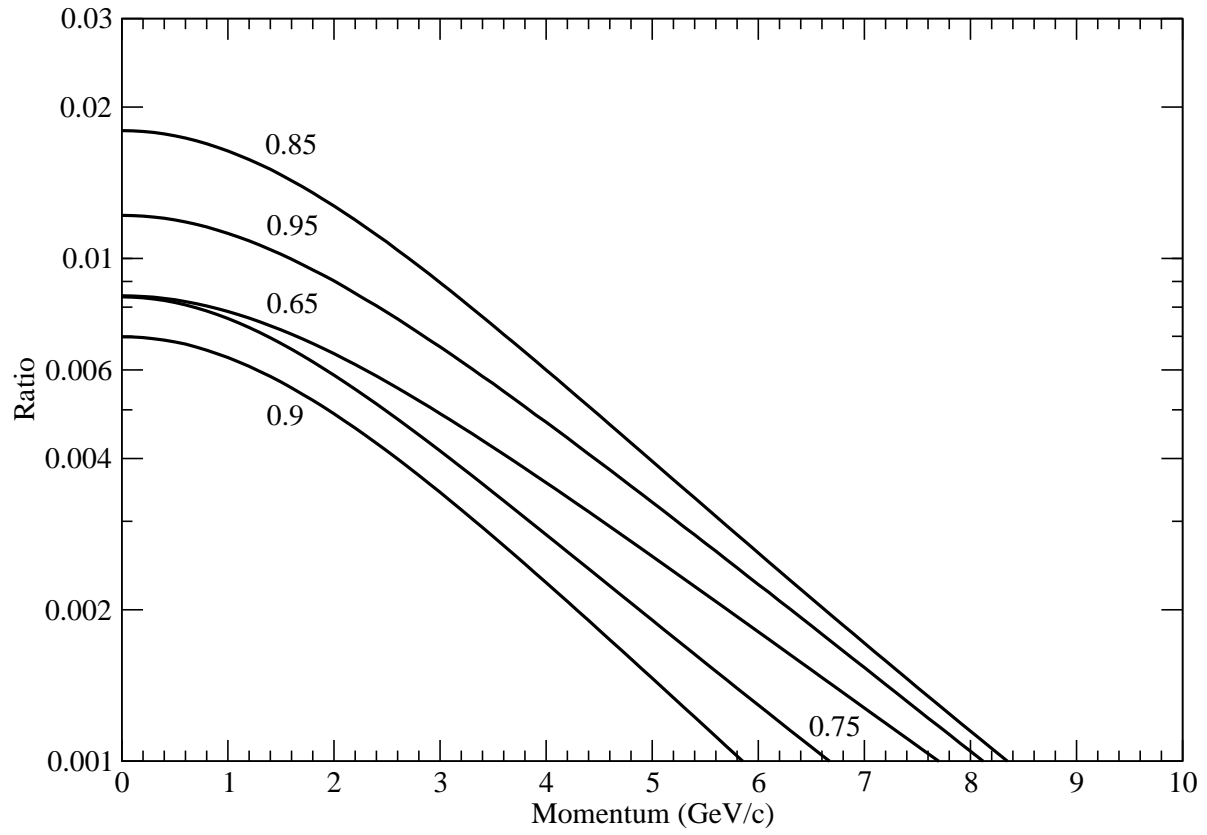


Figure 26: Ratio for $\eta + \psi' \rightarrow \bar{D}^* + D$ and $\pi + \psi' \rightarrow \bar{D}^* + D$ as a function of the ψ' momentum.

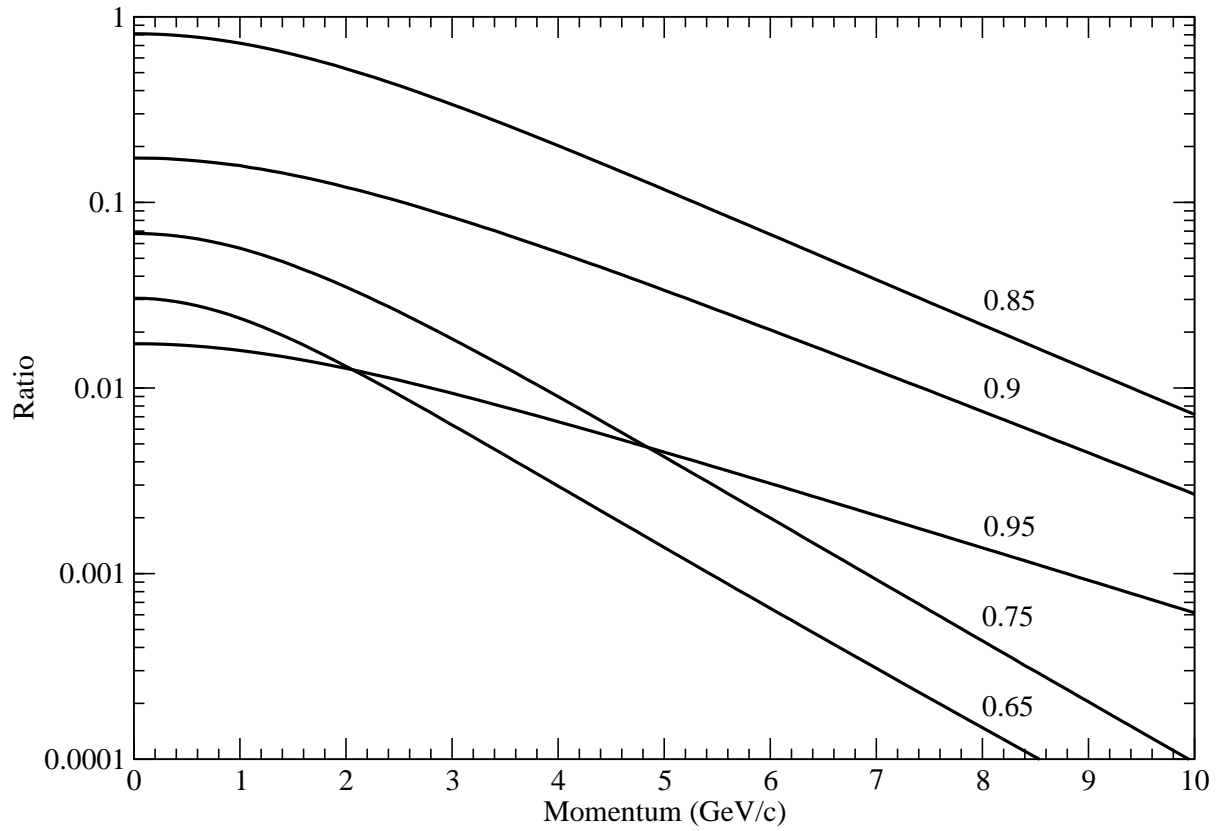


Figure 27: Ratio for $\eta + \psi' \rightarrow \bar{D}^* + D^*$ and $\pi + \psi' \rightarrow \bar{D}^* + D^*$ as a function of the ψ' momentum.

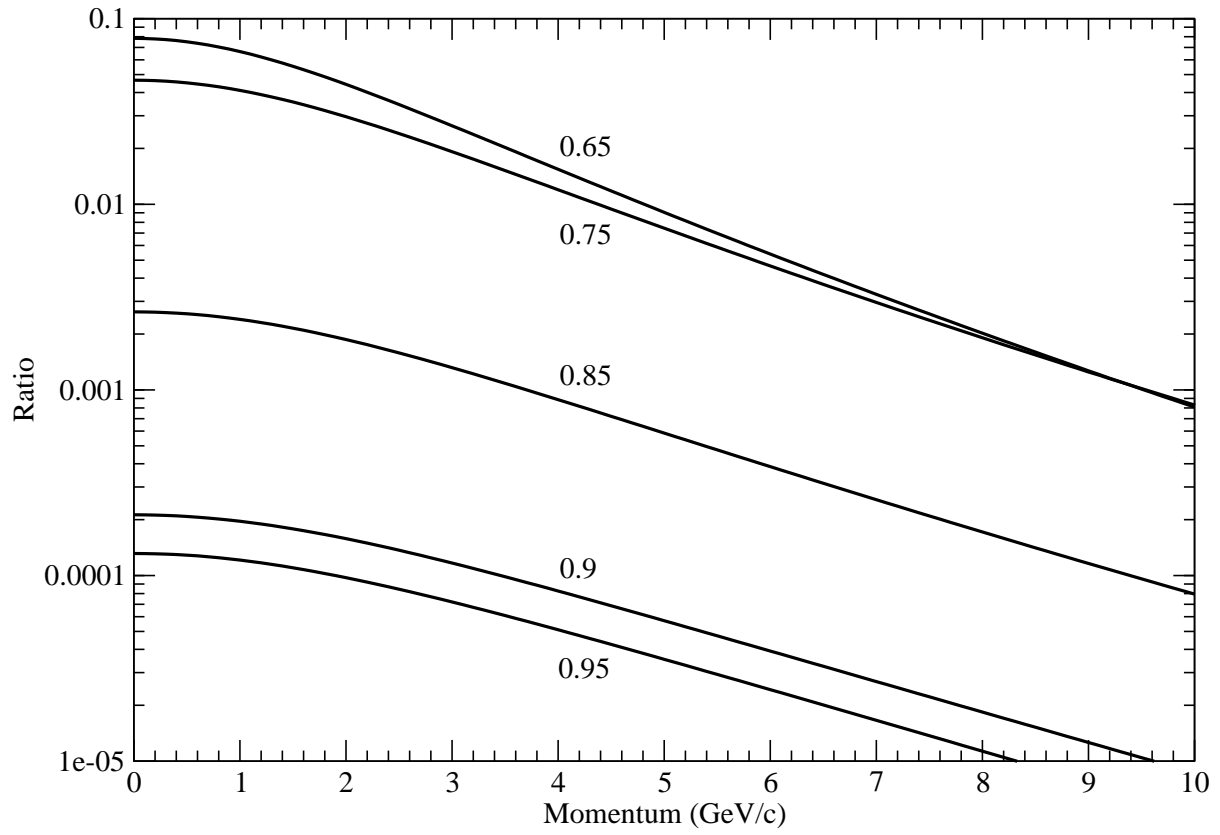


Figure 28: Ratio for $\eta + \chi_c \rightarrow \bar{D}^* + D$ and $\pi + \chi_c \rightarrow \bar{D}^* + D$ as a function of the χ_c momentum.

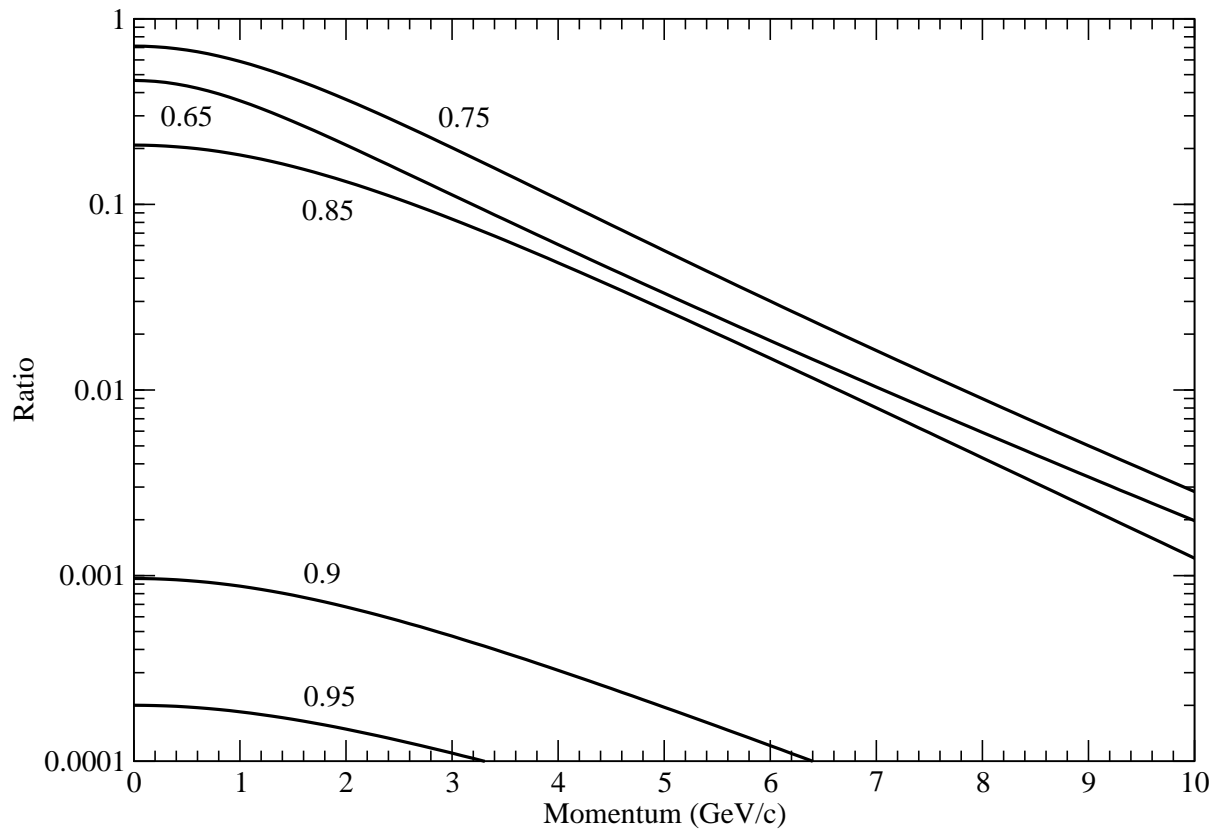


Figure 29: Ratio for $\eta + \chi_c \rightarrow \bar{D}^* + D^*$ and $\pi + \chi_c \rightarrow \bar{D}^* + D^*$ as a function of the χ_c momentum.

Table 1: Quantities relevant to the cross sections for the KJ/ψ dissociation reactions. a_1 and a_2 are in units of mb; b_1 , b_2 , d_0 and $\sqrt{s_z}$ are in units of GeV; c_1 and c_2 are dimensionless.

Reactions	T/T_c	a_1	b_1	c_1	a_2	b_2	c_2	d_0	$\sqrt{s_z}$
$KJ/\psi \rightarrow \bar{D}^* D_s^+$	0	0.27	0.03	0.52	0.1	0.085	2.63	0.044	4.52
	0.65	0.418	0.025	0.52	0.131	0.082	2.58	0.035	4.31
	0.75	0.4	0.012	0.52	0.45	0.06	1.53	0.03	4.18
	0.85	0.27	0.01	0.52	0.34	0.056	1.45	0.03	4.04
	0.9	0.24	0.011	0.44	0.29	0.037	0.74	0.022	3.84
	0.95	0.42	0.019	0.42	0.69	0.01	0.54	0.012	3.52
$KJ/\psi \rightarrow \bar{D} D_s^{*+}$	0	0.22	0.024	0.55	0.12	0.081	2.77	0.04	4.81
	0.65	0.23	0.015	0.55	0.2	0.066	2.06	0.034	4.59
	0.75	0.23	0.009	0.51	0.36	0.048	1.31	0.03	4.41
	0.85	0.235	0.01	0.51	0.29	0.049	1.5	0.029	4.12
	0.9	0.135	0.01	0.48	0.118	0.044	1.2	0.02	3.77
	0.95	0.25	0.007	0.59	0.32	0.011	0.44	0.0091	3.46
$KJ/\psi \rightarrow \bar{D}^* D_s^{*+}$	0	0.0065	0.0179	0.53	0.0376	0.339	4.92	0.3	5.46
	0.65	0.0088	0.075	0.9	0.03	0.27	2.76	0.25	5.17
	0.75	0.0006	0.003	0.36	0.047	0.21	2.47	0.23	4.94
	0.85	0.0092	0.0111	0.5	0.021	0.2158	3.38	0.22	4.54
	0.9	0.0052	0.016	0.46	0.0064	0.21	2.57	0.2	4.31
	0.95	0.215	0.0034	0.52	0.101	0.0134	1.91	0.0047	3.58

Table 2: The same as Table 1 except for the $K\psi'$ dissociation.

Reactions	T/T_c	a_1	b_1	c_1	a_2	b_2	c_2	d_0	$\sqrt{s_z}$
$K\psi' \rightarrow \bar{D}^* D_s^+$	0	0.038	0.014	0.45	0.036	0.214	2.16	0.019	5.12
	0.65	18.3	0.0021	0.42	13.2	0.013	1.13	0.0033	3.93
	0.75	11	0.003	0.45	9.2	0.011	0.93	0.0059	3.82
	0.85	5.52	0.005	0.55	2	0.007	0.39	0.0054	3.68
	0.9	3.4	0.0022	0.47	3.17	0.0089	1.07	0.0053	3.57
	0.95	2.45	0.0019	0.47	1.7	0.0069	1.07	0.0036	3.4
$K\psi' \rightarrow \bar{D} D_s^{*+}$	0	0.043	0.017	0.41	0.033	0.3	4.59	0.015	5.09
	0.65	6.4	0.0075	0.51	1.24	0.019	1.29	0.0091	3.96
	0.75	4.5	0.0039	0.53	2.93	0.016	1.71	0.0072	3.85
	0.85	2.35	0.0036	0.5	0.91	0.0116	1.5	0.0049	3.78
	0.9	1.35	0.0019	0.53	1.01	0.0083	1.55	0.0041	3.59
	0.95	1.45	0.0014	0.5	1.12	0.0056	1.5	0.0029	3.36
$K\psi' \rightarrow \bar{D}^* D_s^{*+}$	0	0.495	0.02	0.63	0.103	0.011	0.29	0.023	5.01
	0.65	2.3	0.005	0.51	1.3	0.018	1.49	0.0084	4.26
	0.75	2.01	0.005	0.49	0.76	0.014	1.1	0.0074	4.07
	0.85	0.445	0.0033	0.51	0.208	0.0132	1.37	0.0055	3.83
	0.9	0.214	0.0031	0.41	0.082	0.0028	0.92	0.0037	3.62
	0.95	1.2	0.0011	0.52	1.11	0.005	1.55	0.0028	3.34

Table 3: The same as Table 1 except for the $K\chi_c$ dissociation.

Reactions	T/T_c	a_1	b_1	c_1	a_2	b_2	c_2	d_0	$\sqrt{s_z}$
$K\chi_c \rightarrow \bar{D}^*D_s^+$	0	0.445	0.104	2.05	0.162	0.035	0.55	0.1	4.77
	0.65	2.55	0.049	1.39	0.83	0.061	0.71	0.05	4.21
	0.75	4.3	0.029	1.21	0.8	0.081	0.62	0.03	4.02
	0.85	3	0.016	0.72	0.73	0.021	2.6	0.018	3.73
	0.9	2.1	0.013	0.65	0.85	0.017	1.66	0.014	3.58
	0.95	1.86	0.01	0.78	0.71	0.021	1.99	0.014	3.38
$K\chi_c \rightarrow \bar{D}D_s^{*+}$	0	0.395	0.102	2.33	0.158	0.041	0.55	0.1	4.98
	0.65	1.5	0.065	1.4	0.66	0.044	1.56	0.059	4.19
	0.75	1.7	0.03	1.4	0.98	0.066	2	0.04	4.04
	0.85	0.72	0.022	1.75	0.62	0.019	0.87	0.02	3.77
	0.9	0.64	0.013	0.86	0.271	0.017	2.32	0.015	3.6
	0.95	1.04	0.014	1.8	0.17	0.005	1	0.013	3.36
$K\chi_c \rightarrow \bar{D}^*D_s^{*+}$	0	0.63	0.09	3.06	0.09	0.03	0.68	0.11	5.22
	0.65	0.645	0.042	1.61	0.152	0.029	0.51	0.04	4.72
	0.75	0.795	0.03	1.36	0.188	0.022	0.45	0.03	4.44
	0.85	0.233	0.0099	0.61	0.103	0.0238	2	0.014	3.97
	0.9	0.1	0.0082	0.69	0.045	0.0114	2.88	0.01	3.73
	0.95	0.59	0.0087	1.11	0.189	0.0139	4.18	0.01	3.37

Table 4: The same as Table 1 except for the $\eta J/\psi$ dissociation.

Reactions	T/T_c	a_1	b_1	c_1	a_2	b_2	c_2	d_0	$\sqrt{s_z}$
$\eta J/\psi \rightarrow \bar{D}^* D$	0	0.2	0.034	0.8	0.343	0.026	0.44	0.03	4.18
or $\bar{D} D^*$	0.65	0.49	0.021	0.46	0.317	0.047	1.2	0.035	4.04
	0.75	0.3	0.013	0.34	0.767	0.038	0.74	0.03	3.94
	0.85	4.7	0.011	0.4	0.517	0.01	2.96	0.01	3.69
	0.9	0.407	0.009	0.6	0.21	0.011	0.4	0.01	3.57
	0.95	0.18	0.008	0.5	0.0167	0.009	1.3	0.01	3.38
$\eta J/\psi \rightarrow \bar{D}^* D^*$	0	0.0213	0.012	0.53	0.022	0.27	9	0.015	5.04
	0.65	0.0547	0.0116	0.53	0.021	0.25	7.1	0.015	4.68
	0.75	0.16	0.017	0.5	0.0113	0.03	3.6	0.02	4.35
	0.85	0.83	0.006	0.48	0.27	0.017	0.62	0.01	3.66
	0.9	1.57	0.006	0.5	0.263	0.011	1.17	0.005	3.48
	0.95	0.407	0.006	0.54	0.043	0.02	1.84	0.005	3.36
$\eta J/\psi \rightarrow D_s^{*-} D_s^+$	0	0.11	0.049	0.7	0.008	0.02	0.2	0.05	4.91
or $D_s^- D_s^{*+}$	0.65	0.147	0.04	0.7	0.0193	0.05	0.23	0.04	4.67
	0.75	0.177	0.039	0.64	0.0053	0.001	0.06	0.04	4.55
	0.85	0.13	0.041	1	0.0347	0.006	0.41	0.03	4.37
	0.9	0.053	0.031	0.71	0.0207	0.02	0.36	0.03	4.21
	0.95	0.033	0.024	0.47	0.008	0.02	0.8	0.02	4.01
$\eta J/\psi \rightarrow D_s^{*-} D_s^{*+}$	0	0.0109	0.042	0.56	0.0293	0.29	5.5	0.25	5.18
	0.65	0.0147	0.034	0.57	0.0307	0.27	3.48	0.24	5.13
	0.75	0.0128	0.041	0.59	0.03	0.26	3.07	0.24	5.09
	0.85	0.00267	0.03	0.56	0.0207	0.18	1.79	0.2	4.82
	0.9	0.00087	0.04	0.55	0.006	0.18	2.03	0.19	4.53
	0.95	0.003	0.16	1.72	0.00087	0.025	0.46	0.13	4.29

Table 5: The same as Table 1 except for the $\eta\psi'$ dissociation.

Reactions	T/T_c	a_1	b_1	c_1	a_2	b_2	c_2	d_0	$\sqrt{s_z}$
$\eta\psi' \rightarrow \bar{D}^*D$	0	0.019	0.18	2.9	0.002	0.013	0.43	0.2	5.47
or $\bar{D}D^*$	0.65	0.033	0.084	1.89	0.0027	0.039	0.6	0.08	4.24
	0.75	0.0293	0.06	1.31	0.0063	0.009	0.51	0.05	4.1
	0.85	0.0053	0.05	1	0.0363	0.01	0.52	0.01	3.81
	0.9	0.0243	0.008	0.5	0.00133	0.07	3.1	0.008	3.63
	0.95	0.0203	0.008	0.51	0.00133	0.02	1.13	0.0075	3.41
$\eta\psi' \rightarrow \bar{D}^*D^*$	0	0.0377	0.0115	0.48	0.0153	0.189	12.5	0.01	5.35
	0.65	2.67	0.0065	0.6	2.33	0.0054	0.45	0.005	3.98
	0.75	1.27	0.002	0.5	1.13	0.008	1.47	0.005	3.81
	0.85	0.203	0.013	1.24	0.167	0.004	0.46	0.01	3.67
	0.9	0.057	0.002	0.55	0.063	0.01	1.51	0.006	3.53
	0.95	0.0257	0.003	0.47	0.0293	0.012	1.14	0.007	3.37
$\eta\psi' \rightarrow D_s^{*-}D_s^{*+}$	0	0.043	0.011	0.46	0.0233	0.25	1.87	0.02	5.13
or $D_s^-D_s^{*+}$	0.65	1.07	0.008	0.4	1.13	0.014	0.89	0.01	4.25
	0.75	0.6	0.011	0.92	0.67	0.008	0.39	0.01	4.14
	0.85	0.233	0.006	0.48	0.193	0.011	0.6	0.01	3.96
	0.9	0.068	0.008	0.63	0.0847	0.013	0.41	0.01	3.81
	0.95	0.0253	0.003	0.37	0.0453	0.02	0.88	0.01	3.68
$\eta\psi' \rightarrow D_s^{*-}D_s^{*+}$	0	0.4	0.01	0.42	0.333	0.025	0.62	0.01	5.03
	0.65	0.333	0.006	0.33	0.513	0.012	1.06	0.01	4.48
	0.75	0.3	0.005	0.44	0.207	0.012	1.14	0.01	4.33
	0.85	0.057	0.004	0.45	0.0153	0.11	6.43	0.01	4.22
	0.9	0.00293	0.005	0.32	0.0093	0.09	4.91	0.07	4.28
	0.95	0.00407	0.054	4.43	0.0014	0.033	0.14	0.05	4.08

Table 6: The same as Table 1 except for the $\eta\chi_c$ dissociation.

Reactions	T/T_c	a_1	b_1	c_1	a_2	b_2	c_2	d_0	$\sqrt{s_z}$
$\eta\chi_c \rightarrow \bar{D}^*D$	0	0.107	0.082	1.1	0.05	0.033	0.5	0.05	4.81
or $\bar{D}D^*$	0.65	0.363	0.03	0.53	0.0267	0.05	3.6	0.03	4.18
	0.75	0.0267	0.069	1.15	0.193	0.02	0.52	0.02	4.05
	0.85	0.00373	0.017	0.43	0.00147	0.005	0.74	0.01	3.86
	0.9	0.000273	0.041	4.08	0.000004	0.001	0.57	0.04	3.73
	0.95	0.0004	0.018	1.71	0.000097	0.003	0.52	0.02	3.38
$\eta\chi_c \rightarrow \bar{D}^*D^*$	0	0.387	0.096	2	0.14	0.035	0.59	0.1	4.89
	0.65	1.57	0.02	0.7	1.83	0.04	1.6	0.03	4.1
	0.75	3.13	0.014	0.66	1.23	0.006	0.4	0.0099	3.93
	0.85	0.12	0.0026	0.52	0.05	0.009	1.61	0.004	3.64
	0.9	0.00035	0.006	0.55	0.000013	0.004	4.4	0.005	3.55
	0.95	0.00053	0.02	2.75	0.00033	0.01	0.58	0.02	3.37
$\eta\chi_c \rightarrow D_s^{*-}D_s^+$	0	0.54	0.11	2.62	0.087	0.038	0.95	0.11	4.94
or $D_s^-D_s^{*+}$	0.65	0.807	0.06	1.55	0.1	0.1	0.56	0.065	4.46
	0.75	0.7	0.05	1.43	0.06	0.02	0.53	0.045	4.25
	0.85	0.213	0.02	0.59	0.0613	0.03	2.2	0.023	3.94
	0.9	0.127	0.014	0.61	0.018	0.018	0.24	0.015	3.81
	0.95	0.0693	0.008	0.55	0.0293	0.019	0.58	0.01	3.62
$\eta\chi_c \rightarrow D_s^{*-}D_s^{*+}$	0	0.08	0.06	4.68	0.087	0.2	0.83	0.08	5.33
	0.65	0.233	0.05	1.36	0.06	0.3	10.52	0.045	5.04
	0.75	0.193	0.04	1.4	0.04	0.28	11.95	0.035	4.79
	0.85	0.0332	0.023	1.48	0.0111	0.24	2.78	0.02	4.42
	0.9	0.0048	0.018	1.49	0.005	0.13	2.39	0.02	4.19
	0.95	0.00257	0.013	1.52	0.00473	0.09	2.02	0.09	3.87